Progress Energy

Serial: NPD-NRC-2010-062 10CFR52.79
August 9, 2010

U.S. Nuclear Regulatory Commission
Attention: Document Control Desk
Washington, D.C. 20555-0001

LEVY NUCLEAR PLANT, UNITS 1 AND 2
DOCKET NOS. 52-029 AND 52-030
REVISION TO FINAL SAFETY ANALYSIS REPORT (FSAR) SECTION 2.4.5, PROBABLE MAXIMUM SURGE AND SEICHE FLOODING, AND SECTION 2.4.6, PROBABLE MAXIMUM TSUNAMI HAZARDS

Ladies and Gentlemen:

Progress Energy Florida, Inc. (PEF) hereby submits voluntary revisions to FSAR Chapter 2 for the Levy Nuclear Plant Units 1 and 2 (LNP). The specific changes identified in the enclosure to this letter will be included in a future revision of the LNP combined license application.

If you have any further questions, or need additional information, please contact Bob Kitchen at (919) 546-6992, or me at (727) 820-4481.

I declare under penalty of perjury that the foregoing is true and correct.

Executed on August 9, 2010.

Sincerely,

John Elnitsky
Vice President
New Generation Programs & Projects

Enclosure

cc : U.S. NRC Region II, Regional Administrator
Mr. Brian C. Anderson, U.S. NRC Project Manager

Progress Energy Florida, Inc.
P.O. Box 14042
St. Petersburg, FL 33733

D094
NRO

NRC Review of Final Safety Analysis Report

PGN RAI ID #: L-0843

PGN Response to NRC RAI:

Progress Energy Florida's (PEF's) response to the Request for Information (RAI) for 02.04.05-08 (LNP-RAI-LTR-040) determined wave runup using the step-by-step approach given in Chapter 4 of the Coastal Engineering Manual (LNP FSAR Reference 2.4.5-219). The RAI response stated that the LNP FSAR would be revised to incorporate the modified Probable Maximum Hurricane (PMH) analysis and results, but did not identify the specific changes. The specific revisions to the LNP COL Application FSAR Section 2.4.5 are identified in this voluntary RAI response. This voluntary RAI response also captures the LNP FSAR changes associated with the response to RAI 02.04.05-04, which also addresses the PMH analyses. The responses to RAIs 02.04.05-04 and 02.04.05-08 were submitted to the NRC by letter dated July 20, 2009 (NPD-NRC-2009-157).

Associated LNP COL Application Revisions:

The text and tables of LNP FSAR Rev 1., Subsection 2.4.5 will be revised as presented below. No changes to references are necessary. Revisions to associated figures are as follows:

- LNP FSAR Rev. 1, Figures 2.4.5-201 through 2.4.5-227 remain unchanged.
- LNP FSAR Rev. 1, Figures 2.4.5-228 through 2.4.5-233 are revised (see Attachments 02.04.05-A through 02.04.05-F).

LNP FSAR Subsection 2.4.5 will be revised to read:

2.4.5 Probable Maximum Surge and Seiche Flooding

2.4.5.1 Probable Maximum Winds and Associated Meteorlogical Parameters

2.4.5.1.1 Historic Storm Surge Events

As stated in FSAR Subsection 2.4.1.1, the LNP is located in southern Levy County, Florida, about 12.8 km (7.9 mi.) east of the Gulf of Mexico. Between 1851 and 2006, northwest Florida was struck by 57 hurricanes. While 14 of these storms were classified as "major hurricanes" (Category 3 or higher), no storms of Category 4 or Category 5 were reported to have struck the area near the LNP site during this time (Reference 2.4.5-201). A list of hurricanes that have impacted the areas within 80 km (50 mi.) of the LNP site from 1867 to 2004 is presented in Table 2.4.5-201 (Reference 2.4.5-202). Figure 2.4.5-201 depicts the hurricane tracks of these storms. Figures 2.4.5-202, 2.4.5-203, 2.4.5-204, 2.4.5-205, 2.4.5-206, 2.4.5-207, 2.4.5-208, 2.4.5-209, 2.4.5-210, 2.4.5-211, 2.4.5-212, 2.4.5-213, 2.4.5-214, 2.4.5-215, 2.4.5-216, and 2.4.5-217 show the tracks of major hurricanes (Category 3 or higher) that impacted the region during each decade from 1850 through 2006.

The coastline of Levy County has a very shallow slope, and this allows hurricane-induced surges to inundate coastal communities (Reference 2.4.5-203). Inglis and Yankeetown are two

residential areas near the LNP site. Analyses of hurricane flood stages for both towns are presented in Table 2.4.5-202. The maximum reported flood elevation for Inglis is 4.3 m (14.2 ft.) above msl (Reference 2.4.5-203). The maximum reported flood elevation for Yankeetown is 6.6 m (21.5 ft.) above msl (Reference 2.4.5-203). The maximum storm surge reported in Levy County from Tropical Storm Frances, which struck land in September of 2004, occurred at Cedar Key and was less than 1.5 m (5 ft.) (Reference 2.4.5-204).

2.4.5.1.2 Probable Maximum Hurricane

As defined by National Oceanic and Atmospheric Administration (NOAA) NWS Report 23 (Reference 2.4.5-205), the PMH is a hypothetical steady-state hurricane having a combination of values of meteorological parameters that will give the highest sustained wind speed that can probably occur at a specified coastal location. A PMH is specified in terms of several meteorological parameters that vary with location: central pressure, peripheral pressure, radius of maximum winds, forward speed, track direction, and inflow angle. Parameters for the PMH analysis are taken from the NOAA NWS Report 23 as shown in Table 2.4.5-203 (Reference 2.4.5-205).

Based on Regulatory Guide 1.59, Revision 2 (1977), the 10 percent exceedence antecedent high spring tide is taken as 1.3 m (4.3 ft.) mean low water (MLW). The maximum astronomical tide (MAT) is 1.5 m (4.9 ft.) mean lower-low water (MLLW), as shown on Figure 2.4.5-218 (Reference 2.4.5-206).

2.4.5.2 Surge and Seiche Water Levels

2.4.5.2.1 Storm Surge Analysis

A storm surge is a temporary rise in sea level caused by water being driven over land primarily by the onshore hurricane force winds and only secondarily by the reduction in sea-level barometric pressure between the eye of the storm and the outer region. The magnitude of the surge at a specific site is also a function of the radius of the maximum hurricane winds, the forward speed of the storm's eye, and the bathymetry near the shoreline.

Three different approaches were used to estimate the storm surge at the LNP site. The first approach was based on using estimates of probable maximum surge levels at open-coast locations computed by the U.S. Nuclear Regulatory Commission (NRC) staff. NUREG-0800, Revision 3 (March 2007) recommends that the PMH surge level should be determined using the data presented in Regulatory Guide 1.59.

The second approach was based on using results obtained by the Evaluation Branch/Meteorological Development Lab, National Weather Service/NOAA/United States Department of Commerce using the Sea, Lake, and Overland Surge from Hurricanes (SLOSH) model (Reference 2.4.5-207) for various categories of hurricanes. Given a group of hypothetical hurricanes of a particular category, speed, and landfall direction, the SLOSH model outputs the maximum storm surge heights at each grid cell in a basin. The SLOSH model results were used to obtain estimates of surge elevations at various locations such as at the coastal line, Yankeetown, Inglis, and near the LNP site due to hypothetical hurricanes of Category 1 through Category 5 impacting the Cedar Key region.

The third approach was based on correlating the estimates of surges at the coastline from the SLOSH model and Hsu's empirical equation (Reference 2.4.5-208) for various categories of hurricanes.

Coastal line surge results obtained from the second and third approaches were used to determine a relationship between these two approaches. The obtained relationship was used to determine the expected PMH surge elevation at the coastal line. Further, the coastal line surge elevations for various categories of hurricanes were related to surge elevations at inland locations such as Yankeetown and Inglis, Florida. These relationships were utilized to determine the PMH surge elevation at the LNP site. Before discussing the PMH and probable maximum surge (PMS) analyses, it is necessary to discuss the datums used for the surge elevation.

There are several datums that have been mentioned in this report. Datums are of two types: tidal and fixed. For example, msl pertains to the local mean sea level (msl), which is a tidal datum as it is based on astronomical tides. A tidal datum is determined over a 19-year National Tidal Datum Epoch. NAVD88 and NGVD29 are fixed geodetic datums whose elevation relationships to local msl and other tidal datums may not be consistent from one location to another. NAVD88 replaced NGVD29 as the national standard geodetic reference for heights. Benchmark elevations relative to NAVD88 are available from National Geodetic Survey (NGS) through the World Wide Web. For the LNP site, the nearest tidal datum is located at the Cedar Key, Florida. Elevations of the Cedar Key tidal datum are defined with respect to tides as given in Table 2.4.5-204 based on 1983 – 2001 epoch (Reference 2.4.5-209).

2.4.5.2.2 PMH Surge Level Determination Using Regulatory Guide 1.59

The NUREG-0800, Revision 3 (March 2007) recommends the storm surge induced by the PMH should be estimated as recommended by Regulatory Guide 1.59 and supplemented by current best practices. Appendix C of Regulatory Guide 1.59 presents timesaving methods of estimating the maximum stillwater level of the PMS from hurricanes at open coast sites on the Atlantic Ocean and Gulf of Mexico. According to Regulatory Guide 1.59, these procedures are based on PMS values determined by the NRC staff and its consultants and by applicants for licenses that have been reviewed and accepted by the NRC staff. Estimates of open-coast stillwater levels at various selected locations are given in Regulatory Guide 1.59. In order to determine estimates of the PMS stillwater level at an open coast site other than these locations, interpolation between these known locations on either side of the site under study can be used after locating it, based on its site-specific bathymetry. The location of the site under study is determined by comparing its ocean profile down to a depth of 182.9 m (600 ft.) MLW to the profiles given in Appendix C of Regulatory Guide 1.59.

In the current analysis, the site under study is very close to Crystal River where a PMS estimate is readily available. Therefore, it can be assumed that the PMS estimate at the coastal line for the LNP site is approximately equal to the open coast PMS estimates for Crystal River. For the open coast location in Crystal River, Table C.1 of Regulatory Guide 1.59 gives the following PMS data:

Wind setup	= 8.09 m (26.55 ft.)
Pressure setup	= 0.81 m (2.65 ft.)

Initial rise	= 0.18 m (0.60 ft.)
10 percent exceedance high tide	= 1.3 m (4.30 ft.) MLW
Total surge	= 10.39 m (34.10 ft.) MLW

Using the above information along with the Cedar Key datum elevation given in Table 2.4.5-204, the PMS estimate at the coastal line for the LNP site is 10.89 m (35.72 ft.) NAVD88.

2.4.5.2.3 Storm Surge Analysis with SLOSH

The second approach for estimating the maximum storm surge at the LNP site is based on results from the SLOSH numerical model corresponding to various categories of hurricanes. SLOSH is a mathematical model that stands for Sea, Lake, and Overland Surge from Hurricanes (Reference 2.4.5-210). SLOSH was developed by the NWS to estimate storm surge heights and winds associated with historical, hypothetical, and predicted hurricanes (Reference 2.4.5-210). SLOSH is the basis for Hurricane Evacuation Studies (HES) and is the primary model used by FEMA, the NOAA, and the USACE (Reference 2.4.5-210).
The National Hurricane Center (NHC) uses the SLOSH model to determine the timing, severity, and sequence of wind and storm surge hazards that can be expected from hurricanes of various intensities, tracks, and forward speeds striking the study area, computing the potential effects of many hundreds of theoretical hurricanes (Reference 2.4.5-211). SLOSH is a mathematical model that cannot perfectly replicate nature. Verification of the SLOSH model was conducted by the NHC with real-time runs of historical storms (Reference 2.4.5-212). The computed surge heights are compared with those measured from historical storms and, if necessary, adjustments are made to the input or basin data. The SLOSH model is generally accurate within plus or minus 20 percent (Reference 2.4.5-213). Based on a statistical analysis conducted by the NHC, adding 20 percent to the computed SLOSH surge values would eliminate most of the potential negative errors. However, such an adjustment would also add additional surge height to those values that already contain positive errors, possibly overestimating the surge heights produced by the SLOSH model.

The point of a hurricane's landfall is crucial to determining which areas will be inundated by the storm surge. If the hurricane forecast track is inaccurate, SLOSH model results will be inaccurate. The SLOSH model, therefore, is best used for defining the potential maximum surge for a location (Reference 2.4.5-213).

Additional features of the SLOSH model output are given below (Reference 2.4.5-210):

- SLOSH can estimate water surface elevations due to the storm surge for both the open coast and on land.

- MEOW: It stands for "Maximum Envelope of Water." Envelope refers to the maximum height the water reaches at any point in time at every grid cell in the SLOSH basin, for a given hypothetical storm. The MEOW is formed from a composite of many individual SLOSH model runs. It is the set of the highest surge values at each grid location for a given storm category, forward speed, and direction of motion, regardless of which individual storm simulation produced the value. The NHC has generated one MEOW for

each storm category, storm direction, forward speed, and tide level used in the simulation study.

- MOM: Maximum of the MEOWs (MOMs) are further combinations of MEOWs. As in the case of MEOWs, the purpose of preparing MOMs is to compensate for forecasting inaccuracies. MOMs are created by the NHC by extracting the highest peak surge values from two or more MEOWs.

- Adjustments to Astronomical Tide: The SLOSH output is a combination of the normal tide and the storm surge to generate the total increase in water level due to a given storm. The SLOSH model accounts for astronomical tides by specifying the initial tide level. In this analysis, the SLOSH model considers an initial mean tide of 2.5 ft. NGVD29. However, the 10 percent exceedance high tide for Cedar Key is 4.3 ft. MLW. The equivalent value of the 10 percent exceedance high tide for Cedar Key in NGVD29 is 2.01 ft. Therefore, the assumed initial tide elevation in the SLOSH model is 0.49 ft. higher than the 10 percent exceedance high tide for the Cedar Key NOAA gauge site. Thus, the SLOSH model output needs to be corrected by subtracting 0.49 ft.

- Adjustments to Wave Effect: The SLOSH model does not provide data concerning the additional heights of waves generated by wind-driven waves on top of the stillwater storm surge.

SLOSH is a two-dimensional finite difference code that uses an adaptive curvilinear grid for various regions along the Gulf and Atlantic coasts. SLOSH assumes uniform friction to solve the equations of motion for reference basins along the Gulf of Mexico and Atlantic Ocean coast. A geographical region with known values for topography and bathymetry is called a SLOSH basin. The individual elements of the SLOSH grid are the basis for calculating water surface elevations caused by storm surge in a specific SLOSH basin. The grid allows for barriers to flow, cuts in barriers, one-dimensional flow in rivers and streams, and increased friction for trees and mangroves in certain grid blocks to be taken into consideration in the calculations. The water depth is calculated based on the elevation of the grid cell and the amount of water that is able to flow into that cell. The water surface is found at the elevation of the water depth combined with the average ground elevation of the grid cell. The SLOSH model contains topographic information for each grid cell. These data are combined with the storm surge calculations based on the storm characteristics to determine the water surface elevations caused by storm surge.

Given a SLOSH basin and a hurricane track (identified by its pressure, radius of maximum winds, location, direction, and speed), the SLOSH model solves a complex set of equations to determine the water surface elevations caused by storm surge. Figure 2.4.5-219 shows the grid for the SLOSH model's Cedar Key Basin, which contains the LNP site location. The parameters for various categories of hurricanes considered in the SLOSH modeling are given in Table 2.4.5-205 (Reference 2.4.5-214).

To determine the surge levels at the coastal line, four different points near the LNP site were selected as shown on Figure 2.4.5-220. Tables 2.4.5-206, 2.4.5-207, 2.4.5-208, and 2.4.5-209 show the maximum surge levels at these locations for each category of hurricane. Table 2.4.5-210 lists the maximum surge levels at these points along with the average of these four surge levels.

Maximum water elevations obtained by the SLOSH model at Yankeetown (29° 1'46.99"N, 82°42'58.00"W) and Inglis (29°1'48.00"N, 82°40'8.00"W) (Reference 2.4.5-215) are given in Table 2.4.5-211.

As is clear from Table 2.4.5-211, the SLOSH MOM scenario predicts that the LNP site is dry for Category 1 through Category 5 hurricanes. The maximum water surface elevations as obtained from the SLOSH model are shown graphically on Figures 2.4.5-221, 2.4.5-222, 2.4.5-223, 2.4.5-224, and 2.4.5-225.

2.4.5.2.4 PMH Surge Level Determination Using Hsu's Empirical Method

The maximum storm surge may be estimated rapidly by modifying Jelesnianski's method (1972) as proposed by Hsu (2004) (References 2.4.5-208, 2.4.5-216, and 2.4.5-217). According to Hsu (Reference 2.4.5-208), the maximum storm surge, *Sp*, can be estimated using the equation:

$$S_P = 0.07(1010 - P_0)F_S F_M \qquad \text{Equation 2.4.5-1}$$

where *Sp* is in meters msl, P_0 is the minimum sea level pressure in millibars (mb), F_S is the shoaling factor (obtained from Figure 2.4.5-226, Reference 2.4.5-208), and F_M is the correction factor for storm motion (from Figure 2.4.5-227, Reference 2.4.5-208). In order to determine F_S, one should know the coastal distance of the shoreline site. The locator map with coastal distances given in NOAA NWS Report 23 (Reference 2.4.5-205), was used to determine the coastal distance of the Cedar Key NOAA gauge site. The coastal distance of the Cedar Key NOAA gauge site is little more than 1931.2 km (1200 mi.). Figure 2.4.5-226 also specifies the location of the Cedar Key NOAA gauge site and its corresponding value of F_S = 1.6. In order to determine F_M, one should know both the forward speed and track direction of the PMH storm. Table 2.4.5-203 lists these parameters for the PMH storm. Using PMH parameters given in Table 2.4.5-203 along with Figure 2.4.5-227, the maximum value of F_M was found to be 0.7. Table 2.4.5-212 presents the PMH parameters used for the Hsu (2004) method.

This technique is of great value, particularly when either a rapid estimation of probable storm surge is needed or areas with limited availability of input data are required for detailed modeling. Using Equation 2.4.5-1, Hsu et al. estimated storm surge heights generated by hurricanes Katrina and Rita in 2005 (Reference 2.4.5-208). Based on comparisons between these estimated and observed surge heights, the surge heights calculated using Equation 2.4.5-1 were found to be in reasonable agreement with preliminary watermark measurements.

The maximum coastal surge heights were calculated using Hsu's empirical equation for various categories of hurricanes. The surge heights estimated using Equation 2.4.5-1 were converted into NGVD29 datum. As is clear from Table 2.4.5-204, the elevation of the Cedar Key NOAA gauge site is 1.24 m (4.06 ft.) NAVD88. Using the VERTCON tool (Reference 2.4.2-202), latitude, longitude, and orthographic height in NAVD88, the corresponding elevation of the Cedar Key NOAA gauge site was found to be 1.443 m (4.733 ft.) NGVD29.

Using this information, a given elevation in msl datum can be converted to NGVD29 datum. For example, an elevation of X ft. msl can be converted into the NGVD29 datum using the following expression:

Elev ft. NGVD29 = X ft. msl + msl Datum (3.84 ft.) - NGVD29 Datum (4.733 ft.)

The above expression can be written as:

Elev ft. NGVD29 = (X ft. msl - 0.893)

After making a datum conversion from msl to NGVD29, surge elevations estimated using Hsu's model were compared with those obtained from the SLOSH model. Table 2.4.5-213 and Figure 2.4.5-228 present this comparison. The data plotted on Figure 2.4.5-228 give the following relationship between the coastline surge elevations resulted by these two different approaches:

$$SLOSH\ Model\ Coastline\ Storm\ Surge\ Elev.\ (ft.\ NGVD29) = 1.07 * Hsu's\ Model\ Coastline\ Storm\ Surge\ Elev.\ (ft.\ NGVD29) + 0.8$$

Equation 2.4.5-2

It is clear from Figure 2.4.5-228 that the maximum storm surge heights at the coastal line for hurricane Category 1 through Category 5, calculated using Hsu's method, are in good agreement with the storm surge heights obtained from the SLOSH model. Thus, Hsu's model can be used to predict the coastline storm surge due to PMH. As indicated in Table 2.4.5-213, the surge elevations estimated using Hsu's model are consistently higher than those obtained from the SLOSH model. Therefore, the surge elevations obtained from Hsu's model are conservative.

Using the results tabulated in Table 2.4.5-210 and Table 2.4.5-211, the coastal storm surge heights and their corresponding water elevations at Yankeetown and Inglis were plotted as shown on Figure 2.4.5-229. This figure suggests that there is a relationship between the open coast surge height and water elevation at a given inland location. Knowing the coastal surge height for a given storm, the water elevation at Yankeetown can be calculated using the following equation:

$$Water\ Elev.\ at\ Yankeetown\ (ft.\ NGVD29) = 1.06 * Coastal\ Surge\ Height\ (ft.\ NGVD29) - 0.02$$

Equation 2.4.5-3

Similarly, the water elevation at Inglis can be calculated using the following equation:

$$Water\ Elev.\ at\ Inglis\ (ft.\ NGVD29) = 1.182 * Coastal\ Surge\ Height\ (ft.\ NGVD29) - 1.9$$

Equation 2.4.5-4

For a given storm, the water elevation at the LNP site can be extrapolated using the following equation:

$$WE_{LNP} = WE_{Yankee} + \frac{(WE_{Inglis} - WE_{Yankee})}{(CD_{Inglis} - CD_{Yankee})}(CD_{LNP} - CD_{Yankee})$$ Equation 2.4.5-5

where, WE_{LNP} and CD_{LNP} are the water elevation (ft. NGVD29) and distance (mi.) of the LNP site from the coastal line, WE_{Yankee} and CD_{Yankee} are the water elevation (ft. NGVD29) and distance (mi.) of Yankeetown from the coastal line, and WE_{Inglis} and CD_{Inglis} are the water elevation (ft. NGVD29) and distance (mi.) of Inglis from the coastal line. Using Equation 2.4.5-5, the water elevation at the LNP site corresponding to the various hurricane storm Category 1 through Category 5 were determined as tabulated in Table 2.4.5-214.

2.4.5.2.5 Determination of Water Elevation at the LNP Site Corresponding to PMH

As shown in Table 2.4.5-203, the PMH parameters vary in a certain range. In order to determine surge elevation, various combinations of probable maximum hurricane parameters were randomly selected using the Monte Carlo Simulation (MCS) technique. Based on 1000 MCS simulations, the coastal surge and water elevations at Yankeetown and Inglis were determined. Using these elevations, water elevations at the LNP site were determined as given on Figure 2.4.5-230. The maximum surge stillwater elevation including 10 percent exceedance high tide was found to be 12.97 m (42.54 ft.).

2.4.5.2.6 Seiches

Seiches are standing waves of a relatively long period that occur in lakes, canals, bays, and on the open coast. According to the USACE, a seiche is defined as (Reference 2.4.5-218):

a. A standing wave oscillation of an enclosed waterbody that continues, pendulum fashion, after the cessation of the originating force, which may have been either seismic or atmospheric.

b. An oscillation of a fluid body in response to a disturbing force having the same frequency as the natural frequency of the fluid system. Tides are now considered to be seiches induced primarily by the periodic forces caused by the Sun and Moon.

Other than the Gulf of Mexico and Lake Rousseau, there are no large bodies of water in the study area. Further, neither of these water bodies are in the immediate vicinity of the LNP site. Additionally, seiche has not been considered as the controlling influence for these bodies of water. Therefore, the potential for flooding at the site due to seiche effects is considered insignificant.

2.4.5.3 Wave Action

2.4.5.3.1 Wave Action and Breaking Wave Setup

As mentioned in FSAR Subsection 2.4.5.2.3, the SLOSH model does not include the additional heights generated by wind-driven waves on top of the stillwater storm surge. Therefore, wind-driven wave height needs to be determined. Within the surf zone, wave breaking is the dominant hydrodynamic process. Waves approaching the coast increase in steepness as water

depth decreases. When the wave steepness reaches a limiting value, the wave breaks, dissipates energy, induces nearshore currents, and results in an increase in water level. This super elevation of mean water level caused by wave action is called wave setup. The most important physical parameter that affects the magnitude of wave setup is the depth of the water on which the surface waves are traveling. In the surf zone, water depth is not a constant; instead it varies with surge stage and ground elevation. These variations in water depth influence wave breaking. The variable water depths can produce major variations in wave conditions over short distances. In order to account for these variations and select the most critical combination of ground elevation and surge elevation, an MCS technique has been used.

Assuming the deep-water depth of 10 m (32.8 ft.), the limiting wave period was determined to be approximately 10 seconds. Further, assuming variation in ground surface elevation from 6.1 m to 7.6 m (20 ft. to 25 ft.) and surge elevation from 12.2 m to 12.8 m (40 ft. to 42 ft.), the wave setup was determined using the step-by-step approach in Chapter 4 of the *Coastal Engineering Manual* (Reference 2.4.5-219). In order to account for the variation in ground surface and surge elevations, both the ground surface and surge elevations were assumed to be uniformly distributed between their ranges. The wave setup was determined by using 1000 random combinations of ground surface and surge elevation to conduct MCS simulations. The maximum wave setup was found to be 1.85 m (6.08 ft.).

2.4.5.3.2 Wave Runup

To calculate wave runup under PMH conditions for the LNP site, the step-by-step approach in Chapter 4 of Coastal Engineering Manual (Reference 2.4.5-219) was used. The same parameters used in the wave setup calculation were used for the wave runup calculation. Further, an MCS simulation was used to incorporate variability in wave runup parameters. Based on the MCS simulation, the maximum wave runup was found to be 0.27 m (0.90 ft.).

The combined effect of wave setup and runup from wind-driven wave action as obtained by 1000 MCS runs is given on Figure 2.4.5-231. It is important to mention that the surge boundary remains on the west side of US Highway 19, which is about 3.2 km (2 mi.) away from the LNP site. Thus, this temporary increase in water level due to wave setup will quickly disperse and it is unlikely to reach to the LNP site.

2.4.5.3.3 Total Water Depth Due to PMH Surge and Wave Action

According to the NRC guidelines, the total potential water depth at the LNP site is the sum of stillwater depth including 10 percent exceedance high tide, wave setup, and wave runup. In order to combine the surge, wave setup, and wave runup, the combined surge and wave action components were incorporated into a single MCS model. The obtained result of the MCS simulation is given on Figure 2.4.5-232. The maximum total water elevation was found to be about 15.10 m (49.52 ft.) NGVD29 or 14.79 m (48.52 ft.) NAVD88. The histogram of the maximum water elevation that indicates the expected probability associated with various water elevations is shown graphically on Figure 2.4.5-233. Additionally, 0.4 ft. and 0.6 ft. were added into the total water elevation to account for potential long-term sea level rise and sea level anomaly, respectively. Thus, including potential long-term sea level rise and sea level anomaly, the PMF elevation is 15.40 m (50.52 ft.) NGVD29 or 15.10 m (49.52 ft.) NAVD88. The results of PMH surge and wave action analysis have been summarized in Table 2.4.5-215.

2.4.5.4 Resonance

The LNP site is located approximately 4.8 km (3 mi.) north of Lake Rousseau and 12.8 km (7.9 mi.) east of the Gulf of Mexico. The adverse effects on the safety-related structures at the LNP site due to the possibility of resonance of oscillations of waves generated either in Lake Rousseau or in the Gulf of Mexico appears unlikely as the resonance induced water column will be quickly dissipated.

2.4.5.5 Protective Structures

All safety-related structures at the plant site are protected from high water levels up to elevation 15.5 m (51 ft.) NAVD88, which is higher than anticipated flood levels due to wave runup associated with the Gulf of Mexico or direct rainfall at the plant site.

LNP COL 2.4-2

Table 2.4.5-201 (Sheet 1 of 2)
Hurricanes within 80.5 Km (50 Mi.) of the LNP Site, Levy County, Florida

	Year	Month	Day	Name	Wind Speed (KTS)	Pressure (Mb)	Category
1	1867	10	6	NOT NAMED	70	NA	H1
2	1871	8	17	NOT NAMED	70	NA	H1
3	1871	8	18	NOT NAMED	70	NA	H1
4	1871	8	25	NOT NAMED	70	NA	H1
5	1871	9	6	NOT NAMED	70	NA	H1
6	1871	9	6	NOT NAMED	70	NA	H1
7	1874	9	28	NOT NAMED	70	NA	H1
8	1878	9	10	NOT NAMED	80	NA	H1
9	1878	9	10	NOT NAMED	90	NA	H2
10	1878	9	10	NOT NAMED	80	970	H1
11	1878	9	10	NOT NAMED	70	NA	H1
12	1880	8	30	NOT NAMED	70	NA	H1
13	1880	10	8	NOT NAMED	70	NA	H1
14	1880	10	8	NOT NAMED	70	NA	H1
15	1882	10	11	NOT NAMED	70	NA	H1
16	1886	7	18	NOT NAMED	70	NA	H1
17	1886	7	19	NOT NAMED	70	NA	H1
18	1888	10	10	NOT NAMED	95	NA	H2
19	1888	10	11	NOT NAMED	95	970	H2
20	1896	9	29	NOT NAMED	110	960	H3
21	1896	9	29	NOT NAMED	100	963	H3
22	1928	9	17	NOT NAMED	110	955	H3
23	1928	9	17	NOT NAMED	90	NA	H2
24	1935	9	4	NOT NAMED	85	NA	H2
25	1935	9	4	NOT NAMED	80	NA	H1
26	1944	10	19	NOT NAMED	65	968	H1
27	1945	6	24	NOT NAMED	80	NA	H1
28	1945	6	24	NOT NAMED	70	NA	H1

Table 2.4.5-201 (Sheet 2 of 2)
Hurricanes within 80.5 Km (50 Mi.) of the LNP Site, Levy County, Florida

	Year	Month	Day	Name	Wind Speed (KTS)	Pressure (Mb)	Category
29	1946	10	8	NOT NAMED	65	NA	H1
30	1949	8	27	NOT NAMED	65	974	H1
31	1950	9	5	EASY	110	NA	H3
32	1950	9	5	EASY	105	958	H3
33	1950	9	5	EASY	105	NA	H3
34	1950	9	5	EASY	100	NA	H3
35	1950	9	6	EASY	85	NA	H2
36	1950	10	18	KING	65	NA	H1
37	1968	10	18	GLADYS	70	NA	H1
38	1968	10	19	GLADYS	70	977	H1
39	1968	10	19	GLADYS	70	978	H1
40	2000	9	17	GORDON	65	985	H1

Notes:
H1 = Category 1 hurricane
H2 = Category 2 hurricane
H3 = Category 3 hurricane
KTS = knots
Mb = millibar
NA = Not available

Source: Reference 2.4.5-202

LNP COL 2.4-2

Table 2.4.5-202
Hurricane Flood Stage Data at Inglis and Yankeetown in Levy County, Florida

Town	Ground Elevation (ft.)	Hurricane Flood Stage Height					
		Cat 5	Cat 4	Cat 3	Cat 2	Cat 1	Tropical Storm
Yankeetown	5	29.7*	25.8*	21.2*	16.3*	10.4*	8.1*
		(21.5)	(17.7)	(13.4)	(8.7)	(2.7)	(0.5)
Inglis	15	31.0*	27.0*	22.1*	15.8*	dry*	dry*
		(14.2)	(10.2)	(5.3)	(dry)	(dry)	(dry)

Notes:
ft. = foot

*Source: Reference 2.4.5-207, Based on 2007 SLOSH Model Output
()Source: Reference 2.4.5-203, Based on Levy County Emergency Management Website

LNP COL 2.4-2

Table 2.4.5-203
Characteristics of the Probable Maximum Hurricane

Parameter	Value		Unit
	Min	Max	
Central Pressure	889	891	Millibars
Peripheral Pressure	1020	1020	Millibars
Radius of maximum winds	6.7	22.3	Nautical miles
Forward speed	16	23	Miles/hour
Maximum wind speed	156	157	Miles/hour
Track Direction	200	245	Degree from North

Source: Reference 2.4.5-205

LNP COL 2.4-2

Table 2.4.5-204
Elevations on Station Datum

Station:	8727520	**T.M.:**	0 W
Name:	Cedar Key, Gulf of Mexico, Fl	**Units:**	Feet
Status:	Accepted	**Epoch:**	1983 – 2001

Datum	Value	Description
MHHW	5.6	Mean Higher-High Water
MHW	5.27	Mean High Water
DTL	3.7	Mean Diurnal Tide Level
MTL	3.85	Mean Tide Level
MSL	3.84	Mean Sea Level
MLW	2.44	Mean Low Water
MLLW	1.8	Mean Lower-Low Water
GT	3.8	Great Diurnal Range
MN	2.83	Mean Range of Tide
DHQ	0.34	Mean Diurnal High Water Inequality
DLQ	0.63	Mean Diurnal Low Water Inequality
HWI	6.49	Greenwich High Water Interval (in Hours)
LWI	0.34	Greenwich Low Water Interval (in Hours)
NAVD	4.06	North American Vertical Datum
Maximum	10.75	Highest Water Level on Station Datum
Max Date	10/7/1996	Date Of Highest Water Level
Max Time	22:48	Time Of Highest Water Level
Minimum	-2.4	Lowest Water Level on Station Datum
Min Date	9/18/1947	Date Of Lowest Water Level
Min Time	11:30	Time Of Lowest Water Level

Notes:
T.M. = time meridian
0 W = 0 west

Source: Reference 2.4.5-209

LNP COL 2.4-2

Table 2.4.5-205
Hurricane Parameters

Hurricane Category Number	Sustained Winds		Atmospheric Pressure in the Eye (millibars)	Storm	Surge	Damage
	(km/h)	(mph)		(meters)	(feet)	Level
1	119 – 153	74 - 95	980	1.2 - 1.5	4.0 - 4.9	Low
2	154 – 177	96 - 110	965 - 979	1.8 - 2.4	5.9 - 7.9	Moderate
3	179 – 209	111 - 130	945 - 964	2.7 - 3.7	8.9 - 12.2	Extensive
4	211 – 249	131 - 155	920 - 944	4.0 - 5.5	13.0 - 18.0	Extreme
5	> 249	> 155	< 920	> 5.5	> 18.0	Catastrophic

Notes:
km/h = kilometer per hour
mph = miles per hour

Source: Reference 2.4.5-214

LNP COL 2.4-2

Table 2.4.5-206 (Sheet 1 of 2)
MOM Surge Heights (Feet NGVD29) at Coastal Point 1, near the LNP Site

Tropical Storm		Category 1		Category 2		Category 3		Category 4		Category 5	
ENE 25	7.9	ENE 25	10	ENE 25	15.6	ENE 25	20.3	ENE 25	24.3	ENE 25	28.9
NE 25	7.9	E 25	9.8	E 25	15.3	E 25	19.9	E 25	23.8	E 25	27.4
E 25	7.6	NE 25	9.2	E 15	14.4	ENE 15	19	ENE 15	23	NE 15	27.3
NNE 25	7.5	E 15	9.1	NE 25	14.4	NE 25	19	NE 15	22.9	ENE 15	27.2
NE 15	6.8	ENE 15	9.1	ENE 15	14.3	E 15	18.9	NE 25	22.9	NE 25	27.1
ENE 15	6.7	NE 15	8.7	NE 15	13.9	NE 15	18.6	E 15	22.6	E 15	26.3
E 15	6.6	NNE 15	7.9	NNE 15	12.7	NNE 15	17.4	NNE 15	21.7	NNE 15	26.3
NNE 15	6.6	NNE 25	7.9	NNE 25	12.5	NNE 25	16.9	NNE 25	20.7	NNE 25	24.8
N 25	6.5	ENE 05	7.7	ENE 05	12.4	ENE 05	16.4	ENE 05	20	ENE 05	23.2
N 15	6	NE 05	7.6	NE 05	12.2	NE 05	16.2	NE 05	19.9	NE 05	23.2
E 05	5.5	E 05	7.4	E 05	11.7	E 05	15.5	E 05	19	E 05	22.2
ENE 05	5.5	NNE 05	7	NNE 05	11.2	NNE 05	15	NNE 05	18.6	NNE 05	21.7
NE 05	5.5	N 05	6.8	N 05	10.8	N 05	14.7	N 15	17.8	N 15	21.4
NNE 05	5.4	N 15	6.4	N 15	10.4	N 15	14.2	N 25	17.4	N 25	21.1
N 05	5.1	N 25	6.1	N 25	9.8	N 25	13.6	N 05	17.3	N 05	19.8
NNW 15	5.1	NNW 05	5.8	NNW 05	9.1	NNW 05	12.2	NNW 05	15	NNW 05	17.8
NNW 05	4.9	NNW 15	5.3	NNW 15	8.4	NNW 15	11.5	NNW 15	14.5	NNW 15	17.6
WNW 05	4	NW 05	4.1	W 15	6	W 15	8.4	W 15	9.2	W 15	9.8
NW 05	3.9	W 05	4	WNW 15	5.2	WNW 15	7.5	WNW 15	8.5	WNW 15	9
W 05	3.9	WNW 05	4	W 05	4.2	W 05	6	W 05	6.9	W 05	7.2

LNP COL 2.4-2

Table 2.4.5-206 (Sheet 2 of 2)
MOM Surge Heights (Feet NGVD29) at Coastal Point 1, near the LNP Site

Tropical Storm		Category 1		Category 2		Category 3		Category 4		Category 5	
NW 15	3.8	NW 15	3.8	NW 15	4.1	NW 15	5.9	NW 15	6.8	NW 15	7.2
W 15	3.6	W 15	3.8	NW 05	4	WNW 05	5.4	WNW 05	6.3	WNW 05	6.7
WNW 15	3.5	WNW 15	3.6	WNW 05	4	NW 05	5.3	NW 05	6.2	NW 05	6.6

Notes:
E = east, W = west, N = north, S = south

Source: Reference 2.4.5-207

LNP COL 2.4-2

Table 2.4.5-207 (Sheet 1 of 2)
MOM Surge Heights (Feet NGVD29) at Coastal Point 2, near the LNP Site

Tropical Storm		Category 1		Category 2		Category 3		Category 4		Category 5	
ENE 25	8	E 25	10.2	E 25	15.9	E 25	20.6	ENE 25	24.9	ENE 25	28.9
NE 25	7.9	ENE 25	10.2	ENE 25	15.9	ENE 25	20.6	E 25	24.5	E 25	28.1
E 25	7.8	E 15	9.4	E 15	14.6	E 15	19.2	NE 25	23.1	NE 25	27.2
NNE 25	7.4	ENE 15	9.2	NE 25	14.5	ENE 15	19.1	ENE 15	23	ENE 15	27.1
ENE 15	6.8	NE 25	9.2	ENE 15	14.4	NE 25	19.1	E 15	22.8	NE 15	27
NE 15	6.8	NE 15	8.6	NE 15	13.8	NE 15	18.5	NE 15	22.7	E 15	26.3
E 15	6.6	NNE 15	7.8	NNE 25	12.6	NNE 15	17.2	NNE 15	21.4	NNE 15	25.9
N 25	6.5	NNE 25	7.8	NNE 15	12.5	NNE 25	16.8	NNE 25	20.7	NNE 25	24.8
NNE 15	6.5	ENE 05	7.6	ENE 05	12.2	ENE 05	16.2	ENE 05	19.7	ENE 05	22.8
N 15	5.9	NE 05	7.4	NE 05	11.9	NE 05	15.9	NE 05	19.5	NE 05	22.7
E 05	5.5	E 05	7.3	E 05	11.6	E 05	15.5	E 05	19.1	E 05	22.3
ENE 05	5.5	NNE 05	6.9	NNE 05	11.2	NNE 05	14.8	NNE 05	18.1	N 25	21.2
NE 05	5.5	N 05	6.7	N 05	10.7	N 05	14.5	N 15	17.6	NNE 05	21.2
NNE 05	5.3	N 15	6.3	N 15	10.2	N 15	13.9	N 25	17	N 15	21.1
N 05	5	N 25	6.1	N 25	9.8	N 25	13.7	N 05	17.2	N 05	19.8
NNW 15	5	NNW 05	5.6	NNW 05	8.7	NNW 05	11.7	NNW 05	14.5	NNW 05	17.2
NNW 05	4.8	NNW 15	5.2	NNW 15	8.3	NNW 15	11.3	NNW 15	14.1	NNW 15	17.1
NW 05	3.9	NW 05	4	W 15	5.9	W 15	8.2	W 15	9	W 15	9.4
W 05	3.9	W 05	4	WNW 15	5.1	WNW 15	7.3	WNW 15	8.3	WNW 15	8.8
WNW 05	3.9	WNW 05	3.9	W 05	4.2	W 05	6.1	W 05	7	W 05	7.3

LNP COL 2.4-2

Table 2.4.5-207 (Sheet 2 of 2)
MOM Surge Heights (Feet NGVD29) at Coastal Point 2, near the LNP Site

Tropical Storm		Category 1		Category 2		Category 3		Category 4		Category 5	
NW 15	3.8	W 15	3.8	NW 15	4.1	NW 15	5.8	NW 15	6.7	NW 15	7.1
W 15	3.6	NW 15	3.7	NW 05	4	NW 05	5.2	NW 05	6.2	NW 05	6.6
WNW 15	3.4	WNW 15	3.6	WNW 05	4	WNW 05	5.2	WNW 05	6.2	WNW 05	6.6

Notes:
E = east, W = west, N = north, S = south

Source: Reference 2.4.5-207

LNP COL 2.4-2

Table 2.4.5-208 (Sheet 1 of 2)
MOM Surge Heights (Feet NGVD29) at Coastal Point 3, near the LNP Site

Tropical storm		Category 1		Category 2		Category 3		Category 4		Category 5	
ENE 25	7.8	E 25	10	E 25	15.6	E 25	20.1	ENE 25	24.2	ENE 25	28
E 25	7.7	ENE 25	9.9	ENE 25	15.5	ENE 25	20	E 25	23.8	E 25	27.5
NE 25	7.7	E 15	9.1	E 15	14.1	E 15	18.6	NE 25	22.5	NE 25	26.4
NNE 25	7.3	NE 25	8.9	NE 25	14.1	NE 25	18.5	ENE 15	22.2	NE 15	26.1
ENE 15	6.6	ENE 15	8.8	ENE 15	13.8	ENE 15	18.4	NE 15	22.2	ENE 15	26
NE 15	6.6	NE 15	8.3	NE 15	13.3	NE 15	18	E 15	22	E 15	25.7
E 15	6.4	NNE 25	7.6	NNE 25	12.3	NNE 15	16.6	NNE 15	20.6	NNE 15	24.8
N 25	6.4	NNE 15	7.4	NNE 15	12.1	NNE 25	16.3	NNE 25	20.2	NNE 25	24.3
NNE 15	6.3	ENE 05	7.2	ENE 05	11.6	NE 05	15.7	E 05	19	NE 05	22.4
N 15	5.8	E 05	7.1	NE 05	11.6	ENE 05	15.5	NE 05	19	E 05	22.2
E 05	5.3	NE 05	7.1	E 05	11.4	E 05	15.4	ENE 05	18.9	ENE 05	22
ENE 05	5.3	NNE 05	6.6	NNE 05	10.8	NNE 05	14.5	NNE 05	17.4	N 25	20.9
NE 05	5.3	N 05	6.4	N 05	10.3	N 05	14	N 15	17	N 15	20.3
NNE 05	5.1	N 15	6.1	N 15	9.9	N 15	13.5	N 25	17	NNE 05	20.3
N 05	4.9	N 25	6	N 25	9.6	N 25	13.5	N 05	16.7	N 05	19.4
NNW 15	4.9	NNW 05	5.4	NNW 05	8.4	NNW 05	11.3	NNW 05	14	NNW 05	16.6
NNW 05	4.7	NNW 15	5.1	NNW 15	8	NNW 15	10.9	NNW 15	13.6	NNW 15	16.3
WNW 05	3.9	NW 05	3.9	W 15	5.7	W 15	7.9	W 15	8.6	W 15	9
NW 05	3.8	W 05	3.9	WNW 15	5	WNW 15	7	WNW 15	8	WNW 15	8.4
W 05	3.8	WNW 05	3.9	W 05	4.2	W 05	5.9	W 05	6.7	W 05	7.1

LNP COL 2.4-2

Table 2.4.5-208 (Sheet 2 of 2)
MOM Surge Heights (Feet NGVD29) at Coastal Point 3, near the LNP Site

Tropical Storm		Category 1		Category 2		Category 3		Category 4		Category 5	
NW 15	3.7	W 15	3.7	NW 15	4	NW 15	5.6	NW 15	6.5	NW 15	6.9
W 15	3.5	NW 15	3.6	NW 05	3.9	NW 05	5.1	NW 05	6	NW 05	6.4
WNW 15	3.4	WNW 15	3.5	WNW 05	3.9	WNW 05	5.1	WNW 05	6	WNW 05	6.3

Notes:
E = east, W = west, N = north, S = south

Source: Reference 2.4.5-207

LNP COL 2.4-2

Table 2.4.5-209 (Sheet 1 of 2)
MOM Surge Heights (Feet NGVD29) at Coastal Point 4, near the LNP Site

Tropical storm		Category 1		Category 2		Category 3		Category 4		Category 5	
ENE 25	7.6	E 25	9.6	E 25	14.5	E 25	19	E 25	23.3	E 25	27.3
NE 25	7.5	ENE 25	9.3	ENE 25	14.3	ENE 25	19	ENE 25	23.2	ENE 25	26.8
E 25	7.5	E 15	8.6	E 15	13.4	E 15	17.8	NE 15	21.9	NE 15	25.9
NNE 25	7.1	NE 25	8.6	NE 25	13.1	NE 15	17.8	NE 25	21.8	E 15	25.7
ENE 15	6.4	ENE 15	8.3	ENE 15	13	NE 25	17.6	E 15	21.7	NE 25	25.6
NE 15	6.4	NE 15	8.0	NE 15	13	ENE 15	17.4	ENE 15	21.1	ENE 15	24.8
E 15	6.3	NNE 25	7.3	NNE 25	11.6	NNE 15	15.9	NNE 15	20	NNE 15	23.8
N 25	6.3	NNE 15	7.1	NNE 15	11.6	NNE 25	15.7	NNE 25	19.8	NNE 25	23.8
NNE 15	6.2	E 05	7.0	E 05	11.3	E 05	15.4	E 05	19.1	E 05	22.2
N 15	5.6	NE 05	7.0	NE 05	11.3	NE 05	15.4	NE 05	18.8	NE 05	22.2
ENE 05	5.2	ENE 05	6.8	ENE 05	10.9	ENE 05	14.7	ENE 05	17.9	ENE 05	21
NE 05	5.2	NNE 05	6.4	NNE 05	10.4	NNE 05	14.1	NNE 05	17.1	N 25	20.6
E 05	5.1	N 05	6.1	N 05	10	N 05	13.5	N 15	16.4	NNE 05	19.9
NNE 05	5.0	N 15	5.9	N 15	9.4	N 15	12.9	N 25	16.4	N 15	19.6
NNW 15	4.8	N 25	5.9	N 25	9.3	N 25	12.8	N 05	16.3	N 05	18.9
N 05	4.7	NNW 05	5.3	NNW 05	8.1	NNW 05	10.8	NNW 05	13.5	NNW 05	15.9
NNW 05	4.6	NNW 15	5.0	NNW 15	7.7	NNW 15	10.4	NNW 15	13	NNW 15	15.6
NW 05	3.8	NW 05	3.8	W 15	5.6	W 15	7.7	W 15	8.4	W 15	9.1
W 05	3.8	W 05	3.8	WNW 15	4.8	WNW 15	6.8	WNW 15	7.8	WNW 15	8.3
WNW 05	3.8	WNW 05	3.8	W 05	4.1	W 05	5.7	W 05	6.6	W 05	6.9

LNP COL 2.4-2

Table 2.4.5-209 (Sheet 2 of 2)
MOM Surge Heights (Feet NGVD29) at Coastal Point 4, near the LNP Site

Tropical Storm		Category 1		Category 2		Category 3		Category 4		Category 5	
NW 15	3.7	W 15	3.7	NW 15	3.9	NW 15	5.4	NW 15	6.3	NW 15	6.6
W 15	3.5	NW 15	3.6	NW 05	3.8	NW 05	4.9	NW 05	5.8	WNW 05	6.2
WNW 15	3.4	WNW 15	3.5	WNW 05	3.8	WNW 05	4.9	WNW 05	5.8	NW 05	6.1

Notes:
E = east, W = west, N = north, S = south

Source: Reference 2.4.5-207

LNP COL 2.4-2

Table 2.4.5-210
Maximum Coastal Line Surge Levels (Feet NGVD29) for Hurricanes of Categories 1 through 5 near the LNP Site

Case	Cat-1	Cat-2	Cat-3	Cat-4	Cat-5
1	10.2	15.9	20.6	24.9	28.9
2	10	15.6	20.3	24.3	28.9
3	10	15.6	20.1	24.2	28
4	9.6	14.5	19	23.3	27.3
Average	10.0	15.4	20.0	24.2	28.3

Notes:
Assumed tide = 2.5 ft. NGVD29.

Source: Reference 2.4.5-207

LNP COL 2.4-2

Table 2.4.5-211
Maximum Water Levels at the LNP Site, Yankeetown, and Inglis Obtained Using the SLOSH Model for Hurricanes of Categories 1 through 5

Category of Hurricane Storm	Water Surface Elevation (Feet NGVD29) Using the SLOSH Model		
	Yankeetown (29° 1'46.99" N, 82°42'58.00" W)	Inglis (29° 1'48.00" N, 82°40'8.00" W)	LNP Site (29° 4'26.72" N, 82°37'14.91" W)
CAT-1	10.40	Dry	Dry
CAT-2	16.30	15.8	Dry
CAT-3	21.20	22.10	Dry
CAT-4	25.80	27.00	Dry
CAT-5	29.70	31.00	Dry

Notes:
Assumed tide = 2.5 ft. NGVD29.

Source: Reference 2.4.5-207

LNP COL 2.4-2

Table 2.4.5-212
PMH Parameters Used for Hsu (2004) Method

Parameter	Value	Unit	Remarks
Central Pressure, P_0	890.4	millibars	Table 2.4.5-204
Shoaling Factor, Fs	1.6	None	Figure 2.4.5-226
Correction Factor, Fm	0.7	None	Figure 2.4.5-227
Storm Surge Height, Sp	30.76	feet msl	Equation 2.4.5 1

Source: References 2.4.5-217, 2.4.5-205, 2.4.5-208

LNP COL 2.4-2

Table 2.4.5-213
Coastline Storm Surges for Category 1 through 5 Hurricanes

	Storm Surge Height (Feet NGVD29)	
Hurricane Storm Category	Hsu Method	SLOSH Model
1	9.7	9.5
2	11.8	14.9
3	16.3	19.5
4	22.1	23.7
5	25.2	27.8

Notes:
SLOSH model results presented in FSAR Table 2.4.5-210 were corrected for 10% high tide of 2.01 ft. NGVD29.

LNP COL 2.4-2

Table 2.4.5-214
Determination of Water Elevation at the LNP Plant Site by Extrapolation for Hurricanes of Categories 1 through 5

Location	Ground Elev. (ft.)	Distance from Sea (mi.)	Cat-1	Cat-2	Cat-3	Cat-4	Cat-5
Yankeetown	5	2.4	9.9	15.8	20.7	25.3	29.2
Inglis	15	5.97		15.3	21.6	26.5	30.5
Plant Site	51	8.5		15.0	22.2	27.4	31.4

Notes:
All elevations are in feet NGVD29. The nominal plant grade elevation is 50 ft. NAVD88 (51 ft. NGVD29).
ft. = foot, mi. = mile

LNP COL 2.4-2

Table 2.4.5-215
Results Summary

Item	Elevation NGVD29 (Ft.)	Elevation NAVD88 (Ft.)
LNP grade elevation	51	50
10% exceedance high tide	2.01	1.01
PMH storm surge w/o wind action including 10% exceedance high tide	42.54	41.54
Additional wind driven wave heights (wave setup)	6.08	6.08
Additional wind driven wave heights (wave runup)	0.90	0.90
Adjustment to long-term sea level rise	0.40	0.40
Sea Level Anomaly	0.60	0.60
Total PMH surge including wave effects	50.52	49.52

Notes:
At the LNP site, NAVD88 (ft.) = NGVD29 (ft.) - 1 ft.

Attachments/Enclosures:

Attachment 02.04.05-A	Figure 2.4.5-228: Comparison of Maximum Storm Surge Heights Using HSU Method and SLOSH Model
Attachment 02.04.05-B	Figure 2.4.5-229: Relationship Between the Coastal Storm Surge Heights and Water Elevations
Attachment 02.04.05-C	Figure 2.4.5-230: Water Elevation at LNP Site Due to PMH-Induced Surge as Indicated by 1000 Monte Carlo Simulation Runs
Attachment 02.04.05-D	Figure 2.4.5-231: Wave Setup and Runup Due to Wind-Driven Wave Action as Indicated by 1000 Monte Carlo Simulation Runs
Attachment 02.04.05-E	Figure 2.4.5-232: Total Water Elevation at LNP Site Due to PMH-Induced Surge and Wave Action as Indicated by 1000 Monte Carlo Simulation Runs
Attachment 02.04.05-F	Figure 2.4.5-233: Histogram of Total Water Elevation at LNP Site Due to Wave Setup, Runup, and PMH-Induced Surge as Indicated by 1000 Monte Carlo Simulation Runs

NRC Review of Final Safety Analysis Report

PGN RAI ID #: L-0844

PGN Response to NRC RAI:

Progress Energy Florida's (PEF's) response to the Request for Information (RAI) for 02.04.06-08 (LNP-RAI-LTR-047) presented the analysis procedure used to calculate tsunami wave height at the LNP site, initial tsunami size, propagation, runup, and inundation specific to the LNP site, along with its theoretical basis, assumptions, and source parameterization. The RAI response stated that the LNP FSAR would be revised to incorporate the modified Probable Maximum Tsunami (PMT) analysis and results, but did not identify the specific changes in all cases. The specific revisions to the LNP COL Application FSAR Subsection 2.4.6 are identified in this voluntary RAI response. This RAI response captures the LNP FSAR changes associated with the response RAIs 02.04.06-08 and 02.04.06-10 submitted to the NRC by letter dated July 22, 2009 (NPD-NRC-2009-147) and the responses to RAIs 02.04.06-11, 02.04.06-13, and 02.04.06-14 submitted to the NRC by letter dated March 25, 2010 (NPD-NRC-2010-025).

In addition, the FSAR changes associated with the supplemental response to RAI 02.04.06-15 (submitted to the NRC by letter dated July 19, 2010; NPD-NRC-2010-061) regarding the Probable Maximum Tsunami (PMT) are also reflected in this voluntary RAI.

Associated LNP COL Application Revisions:

The text, tables, and references of LNP FSAR Rev 1., Subsection 2.4.6 will be revised as presented below. Revisions to associated figures are as follows:

- LNP FSAR Rev. 1, Figures 2.4.6-201 through 2.4.6-227 remain unchanged.
- LNP FSAR Rev. 2, Figures 2.4.6-228 and 2.4.6-229 are added (see Attachments 02.04.06-A and 02.04.06-B).

LNP FSAR Subsection 2.4.6 will be revised to read:

2.4.6 Probable Maximum Tsunami Hazards

2.4.6.1 Probable Maximum Tsunami

According to the NRC:

> The probable maximum tsunami (PMT) is defined as that tsunami for which the impact at a site is derived from the use of best available scientific information to arrive at a set of scenarios reasonably expected to affect the nuclear power plant site taking into account: (a) appropriate consideration of the most severe of the natural phenomena that have been historically reported or determined from geological and physical data for the site and surrounding area, with sufficient margin for the limited accuracy, quantity, and period of time in which the historical data have

been accumulated, (b) appropriate combinations of the effects of normal and accident conditions with the effects of the natural phenomena, and (c) the importance of the safety functions to be performed (Reference 2.4.6-201).

2.4.6.2 Historical Tsunami Record

Tsunamis are ocean waves generated either by seismic events (such as large earthquakes) or nonseismic disturbances (such as volcanic eruptions or landslides) that occur near or under the ocean. Based on the United States historical tsunami record (Reference 2.4.6-201), tsunamis were induced by:

- Earthquake (71 percent).
- Landslides triggered by earthquakes (13 percent).
- Landslides (10 percent).
- Volcano Eruptions (2 percent).
- Others (4 percent).

These waves, generally characterized by an extremely long wavelength and period, travel out of the area of their origin and can be extremely dangerous and damaging when they reach the shore. As tsunamis are relatively rare, instrumentation dedicated to collecting tsunami data has been slow to be developed. Tide gauges were developed in the 1850s and the first tsunami was recorded on the U.S. West Coast in 1854, after having been generated in Japan (Reference 2.4.6-202).

As noted, the vast majority of tsunamis are produced by earthquakes. The magnitude of an earthquake is a logarithmic measure of the amount of energy released in the form of seismic waves from its epicenter (Reference 2.4.6-203). Magnitude is a useful measure for characterizing earthquakes that are likely to produce destructive tsunamis. However, there are multiple scales used to measure the magnitude of an earthquake, and the following three have been referenced in the literature reviewed for this report: local magnitude (M_L), surface-wave magnitude (M_s), and moment magnitude (M_w).

Local magnitude, also known as the "Richter magnitude," describes the logarithmic relationship between earthquake size and observed peak ground motion (Reference 2.4.6-204). Based on either S-waves or surface-waves, the local magnitude is generally measured at distances less than 600 km (370 mi.) and depths less than 70 km (43 mi.) (Reference 2.4.6-203). Surface-wave magnitude is a scale based on ground roll waves (a.k.a., Rayleigh waves), and it is useful for more distant observations (Reference 2.4.6-204). Surface-wave magnitude can be determined for earthquakes that are located at distances between 20 and 160 geocentric degrees from a recording station, have a seismic-wave period between 18 and 22 seconds, and have a depth less than 50 km (31 mi.). The moment magnitude is usually similar in value to the surface-wave magnitude. The moment magnitude is a function of the rupture area, fault offset or "slip," and rock strength (as measured by the shear modulus, μ) associated with the earthquake source (Reference 2.4.6-203).

2.4.6.2.1 Sources of Historic Tsunami Data

To summarize the historical tsunamis that affected the gulf coasts of the United States, various sources were explored for relevant information on tsunami-generating sources and wave height and runup events. These data sources include primarily the National Geophysical Data Center (NGDC) tsunami database, Science of Tsunami Hazards journal archives, the USGS, the NOAA Center for Tsunami Research and published literature on historical Caribbean tsunamis.

The maximum height a tsunami reaches on shore is known as the "runup." This is the vertical difference between the msl surface and the maximum height reached by the water on shore. A tsunami is considered particularly dangerous if the resulting runup exceeds 1 m (3.28 ft.). The magnitude of runup is dependent on several factors including how the tsunami's energy is focused at the point of impact, the tsunami's travel path, coastal configuration in the region of impact, and offshore topography. In general, land with steep coastal slopes or barrier reefs experience very little runup, and are only at moderate risk from tsunamis (Reference 2.4.6-205).

The NGDC tsunami database (Reference 2.4.6-206) is a listing of historical tsunami source events and runup locations throughout the world that range in date from 2000 B.C. to the present. The events were gathered from scientific and scholarly sources, regional and worldwide catalogs, tide gauge reports, individual event reports, and unpublished works. In this database, there are currently over 1700 source events. The global distribution of these events is 71 percent Pacific Ocean, 11 percent Mediterranean Sea, 9 percent Atlantic Ocean and Caribbean Sea, 6 percent Indian Ocean, and 3 percent Black Sea. There are over 9600 runup locations where tsunami effects were observed. The global distribution of these locations is 82 percent Pacific Ocean, 6 percent Atlantic Ocean and Caribbean Sea, 3 percent Mediterranean, 9 percent Indian Ocean, and <1 percent in the Red Sea and Black Sea (Reference 2.4.6-206).

The USGS has published a fact sheet on improving earthquake and tsunami warnings for the Caribbean Sea, the Gulf of Mexico, and the Atlantic Coast that includes a map showing the seismology and tectonic setting of the Gulf Coast and Caribbean Region from 1530 to 1991 (Reference 2.4.6-207). The map is reproduced on Figure 2.4.6-201 and it shows the locations of historic earthquake epicenters and the tectonic plate boundaries in the region. NOAA's Center for Tsunami Research, in conjunction with the Pacific Marine Environmental Laboratory, has developed a database that includes worldwide event monitoring and numerical model simulations. NOAA's database includes recent tsunami events (Reference 2.4.6-208). Finally, the publication titled, "A Brief History of Tsunamis in the Caribbean Sea," is a compendium of data and anecdotal material on tsunamis reported in the Caribbean from 1498 to 1997 (Reference 2.4.6-209). Similar historical tsunami events during 1668 to 1998 have been documented elsewhere (Reference 2.4.6-210).

2.4.6.2.2 Observed Historic Tsunami Events Impacting the Caribbean

Reference 2.4.6-209 gives an overview of the tsunami history from 1498 to 1997 in the Caribbean Sea in terms of source events and runup elevations illustrating future expected

geologic hazards. Based on this document, tsunamis are a relatively minor hazard in the Caribbean. The record for the last hundred years lists 33 possible tsunamis or 1 about every 3 years. It was observed that the typical recurrence interval for the destructive tsunamis in the Caribbean is about 21 years. The last destructive tsunami in the Caribbean occurred in August 1946, more than 60 years ago. Wave heights of 2.5 m (8.2 ft.) at Matancitas and 4 to 5 m (13.1 to 16.4 ft.) at Julia Molina were reported (Reference 2.4.6-209). This tsunami was generated by an M_s = 7.8, M_w = 8.1 earthquake that occurred about 65 km (40.4-mi.) off the northeast coast of the Dominican Republic. The waves produced by this tsunami were recorded at Daytona Beach, Florida, at Atlantic City, New Jersey, and at Bermuda. The travel time from the earthquake epicenter to Atlantic City was 4.8 hours, and 4.0 hours for Daytona Beach. An aftershock that occurred 4 days later produced a small tsunami that impacted the same areas (Reference 2.4.6-210).

In the Caribbean, there are four source mechanisms that have produced tsunamis in the past: tsunamis from remote sources (teletsunamis), tsunamis generated by mass movements (landslide tsunamis), tsunamis generated by volcanic processes (volcanic tsunamis), and tsunamis produced by earthquakes (tectonic tsunamis) (Reference 2.4.6-209). Table 2.4.6-201 lists verified historic Caribbean tsunamis from 1498 to 2000 in terms of their origin and impacted locations (Reference 2.4.6-209). Based on this data, it can be stated that historically no Caribbean tsunami has impacted the United States Gulf Coast. Thus, it is unlikely that any tsunami generated in the Caribbean Sea will impact the Gulf Coast of northern-central Florida where the LNP site is located.

2.4.6.2.3 Observed Historic Tsunami Events Impacting the Gulf Coast

In the recorded history, tsunami waves recorded along the Gulf Coast have all been less than 1 m (3.28 ft.) (Reference 2.4.6-211). Tables 2.4.6-202 and Table 2.4.6-203 list various tsunami events that have affected the Caribbean and gulf coasts, respectively, as indicated by the NGDC tsunami database (Reference 2.4.6-206). These records include a tsunami event generated by the 1964 Gulf of Alaska earthquake. Though this event was recorded in both Louisiana and Texas, the waves that impacted these locations are technically termed a "seiche." As defined in FSAR Subsection 2.4.5.2.6, a seiche is an oscillation of a water body and is most commonly recognized in tsunamis as a standing wave. Though most often caused by atmospheric disturbances, they can also be generated by the ground motion associated with earthquakes. There are multiple early 20th-century reports of tsunami waves from Caribbean earthquakes along the Gulf Coast that are difficult to evaluate, but in each case, the maximum wave heights generated appeared to be less than 1 m (3.28 ft.) (Reference 2.4.6-211).

Three historical tsunamis have been documented for the Gulf Coast in the available tsunami databases and literature referenced above. The first of these tsunami events occurred on October 24, 1918, when a small wave was recorded at the Galveston, Texas, tide gauge. This tsunami was presumed to be the result of an aftershock of an October 11, 1918, earthquake (Reference 2.4.6-209). The M_s = 7.5, M_w = 7.3 earthquake originated in the Mona Passage, approximately 15 km (9.3 mi.) northwest of Puerto Rico (Reference 2.4.6-210). It was likely the result of subduction activity in the Brownson Deep. The initial earthquake produced a tsunami that reached a runup height of 6 m (19.7 ft.), and caused significant damage in Puerto Rico (Reference 2.4.6-209). The October 24 tsunami event has a validity rating in the NGDC database of four on a scale from zero to four, where

zero and one are used for erroneous or very doubtful events, respectively, and four is used for definite events (Reference 2.4.6-209). The magnitude of the runup of this tsunami in the Gulf Coast was not reported.

The second documented tsunami event in the Gulf occurred on May 2, 1922 (Reference 2.4.6-209). The epicenter of the earthquake associated with this event was near Isla de Vieques, Puerto Rico. Four hours after the occurrence of the earthquake, a wave with an amplitude of 0.6 m (1.97 ft.) was reported on a tide gauge at Galveston, Texas. A train of three waves with a 45-minute period that were followed 8 hours later by a similar train of smaller waves was observed (Reference 2.4.6-209). However, the validity rating of this event in the NGDC database is a two (i.e., doubtful). The magnitude of the 1922 earthquake and the aftershock has not been estimated.

The third reported tsunami event that impacted the Gulf occurred on March 27, 1964, and was recorded throughout the Gulf of Mexico (Reference 2.4.6-206). This event coincided with the 1964 Alaska earthquake (M_w = 9.2) earthquake that originated in Prince William Sound, Alaska (Reference 2.4.6-212). The earthquake resulted in a vertical displacement ranging from 11.5 m (37.7 ft.) of uplift to 2.3 m (7.5 ft.) of subsidence over more than 520,000 km^2 (200,800 $mi.^2$) of land in the region of origin. While 15 people were killed in the initial earthquake, another 110 lost their lives in the tsunami that followed. The maximum wave height measured was 67 m (220 ft.) at Valdez Inlet. The majority of tsunami damage occurred in the Gulf of Alaska and along the west coast of the United States. According to the USGS, the resultant "Seiche action in rivers, lakes, bayous, and protected harbors and waterways along the Gulf Coast of Louisiana and Texas caused minor damage" (Reference 2.4.6-212). The validity of this event is a four (Reference 2.4.6-206).

2.4.6.3 Source Generator Characteristics

2.4.6.3.1 Tsunamigenic Source Mechanisms

Historically, 71 percent of tsunamis striking the United States have been induced by earthquakes (Reference 2.4.6-201). Considering all source mechanisms, the most destructive tsunamis are the result of large, shallow earthquakes with an epicenter or fault line near the ocean floor. Large earthquakes can tilt, offset, or otherwise displace large areas of ocean floor for distances ranging from a few kilometers to 1000 km (621 mi.) or more. When large vertical offsets occur, these earthquakes also displace water and produce destructive tsunami waves. Tsunami waves can travel large distances from their source. For example, in 1960, there was an earthquake off the coast of Chile with a magnitude of M_W = 9.5 (M_S = 8.6) and a rupture zone of 1000 km (621 mi.). This earthquake produced the Great 1960 Chilean tsunami, as well as destructive waves that hit Hawaii, Japan, and other locations in the Pacific (Reference 2.4.6-205).

Though less common, tsunami events can also result from rock falls, icefalls, and sudden submarine translational landslides or rotational slumps (Reference 2.4.6-205). Historically, 23 percent of tsunamis striking the United States have been the result of landslides (Reference 2.4.6-201). These events are caused by sudden failures of submarine slopes, which are often triggered by earthquakes. In the 1980s, construction work along the coast of Southern France triggered an underwater landslide that produced destructive tsunami waves in the harbor of Thebes (Reference 2.4.6-205). It is also thought that a 1998

earthquake triggered a large underwater slump of sediments, which produced a tsunami that destroyed coastal villages and killed thousand of people along the northern coast of Papua, New Guinea.

Volcano-induced tsunamis are rare, and account for only about 2 percent of tsunami events impacting the United States (Reference 2.4.6-201). However, like landslides, volcanic eruptions are impulsive disturbances, and they are capable of displacing large volumes of water and producing extremely destructive tsunami waves in the area in close proximity to their source. Volcanoes can produce tsunamis by one of three methods. According to the International Tsunami Information Center, "waves may be generated by the sudden displacement of water caused by a volcanic explosion, by a volcano's slope failure, or more likely by a phreatomagmatic explosion and collapse/engulfment of the volcanic magmatic chambers." The 1883 explosion and collapse of the Indonesian volcano Krakatoa produced one of the largest and most destructive tsunamis ever recorded. The resulting tsunami waves reached a height of 41.15 m (135 ft.), and resulted in significant damage to property and loss of human life. A similar explosion and collapse of the volcano Santorin in the Aegean Sea may have produced a tsunami that destroyed Greece's Minoan civilization in 1490 B.C. (Reference 2.4.6-205).

Most meteorites burn up within the atmosphere and no asteroid has fallen during recorded history. However, large craters are evidence that large meteorites have struck the Earth's surface in ancient history, and it is possible that a large asteroid fell on Earth sometime during the Cretaceous period, 65 million years ago. Given that water covers four-fifths of the planet's surface, falling asteroids and meteorites have a good chance of impacting oceans and seas. According to the International Tsunami Information Center, "The fall of meteorites or asteroids in the earth's oceans has the potential of generating tsunamis of cataclysmic proportions." The impact of a moderately sized asteroid, 5 to 6 km (3.1 to 3.7 mi.) in diameter, in the Atlantic Ocean could produce a tsunami that would destroy Atlantic Coast cities and travel to the Appalachian Mountains in the northern two-thirds of the United States (Reference 2.4.6-205). Meteorites and asteroids are potential tsunamigenic sources; however, the occurrence of such an event is highly unlikely.

It is believed that a large nuclear explosion could also serve as a tsunamigenic source. However, no significant tsunami has been reported as the result of nuclear testing, which is currently banned by international treaty (Reference 2.4.6-205).

2.4.6.3.2 Locations of Tsunamigenic Sources

Two historic tsunamigenic sources have been observed and documented in the Gulf of Mexico. The historic tsunamigenic sources include seismic events originating in the North Caribbean Sea and in the Aleutian Trench in Alaska (Reference 2.4.6-206). In addition, simulations indicate that an historic earthquake originating in the Azores-Gibraltar fracture zone (near Lisbon, Portugal), may have also produced a tsunami that reached the Gulf Coast (Reference 2.4.6-213). All three of these sources are far-field sources, or more than 1000 km (620 mi.) from the Levy County coastline.

According to a recent report prepared by the USGS for the NRC (Reference 2.4.6-214), far-field submarine landslides may also be potential tsunamigenic sources. However, local tsunamis are generally much more destructive than tsunamis generated from a distant

source. In addition, they may occur within minutes of the earthquake or landslide that produces them, allowing little time for evacuation. Both the Caribbean region and the Gulf of Mexico provide potential local tsunamigenic sources, as discussed in detail in the following subsections.

2.4.6.3.2.1 Tsunamigenic Sources in the Caribbean

As shown on Figure 2.4.6-202, the Caribbean region, in particular, is characterized by high seismic activity and is prone to strong, shallow earthquakes capable of generating tsunamis (Reference 2.4.6-215). This may occur as a result of the movement of the Caribbean plate. The Caribbean plate underlies a region bounded by Honduras, Nicaragua, Costa Rica, Panama, Colombia, Venezuela, the Lesser Antilles, Puerto Rico, Hispaniola, and Jamaica. The plate moves semi-independently of its surrounding plates, which include the North American, South American, and Cocos plates (Figure 2.4.6-203) (Reference 2.4.6-209). As the Caribbean plate moves eastward (and slightly north of eastward), the two American plates are driven under, or subducted, beneath its eastern edge. This process has produced a chain of active volcanoes along the Lesser Antilles, which may also prove to be an additional tsunamigenic source. In addition, the Cocos plate is moving northeastward and is being subducted beneath the western edge of the Caribbean plate. The strain of the Caribbean plate against the surrounding plates results in a band of high earthquake potential that surrounds the plate (Reference 2.4.6-209). The type of vertical displacement of the ocean floor necessary for the generation of a tsunami event can readily occur in this region (Reference 2.4.6-215).

The Caribbean Sea is bordered in the east by the Lesser Antilles islands, an active volcanic island arc and potential tsunamigenic source. Large submarine landslides are also potential tsunamigenic sources in the Caribbean Sea (Figure 2.4.6-204) (Reference 2.4.6-207). Many of the Caribbean islands are characterized by steep slopes in relatively shallow waters, and are prone to submarine slides and slumps as a result (Reference 2.4.6-215). In particular, side-scan sonar has revealed unusual submarine formations north of Puerto Rico, which are likely the result of slumping. Such events are capable of producing destructive tsunamis (Reference 2.4.6-209).

2.4.6.3.2.2 Tsunamigenic Sources in the Gulf of Mexico

Though no documented tsunami has originated within the Gulf of Mexico (Reference 2.4.6-206), potential tsunamigenic sources exist. In particular, the southern portion of the Gulf of Mexico is characterized by historic seismic activity (Figure 2.4.6-201). According to the USGS National Earthquake Information Center, earthquakes originating beneath the center of the Gulf of Mexico have also been reported. In the past 30 years, more than a dozen such events have been recorded from the eastern Gulf of Mexico. The most recent of these occurred on September 10, 2006, originating 405 km (250 mi.) south-southwest of Apalachicola, Florida (26.331°N, 86.577°W). This earthquake had a magnitude of M_W = 5.8, and is the largest on record for the eastern Gulf of Mexico. Though the quake caused no damage to life or property, it was felt in parts of Florida, Georgia, Alabama, Kentucky, Louisiana, Mississippi, North Carolina, South Carolina, Tennessee and Texas, as well as in the Bahamas and at Cancun and Merida, Mexico (Figure 2.4.6-205). The earthquake also produced seiches in swimming pools in Florida. Prior to the September

quake, the region's last similar quake occurred on February 10, 2006, with a magnitude of $M_W = 5.2$ (Reference 2.4.6-216).

Though the Gulf of Mexico is characterized by frequent landslide events, they have not been a source of tsunamis that have been documented instrumentally or in the geologic record for the Gulf Coast (Reference 2.4.6-206). However, in the 1960s, the petroleum industry discovered a large, potentially tsunamigenic, submarine slump site in the northwest corner of the Gulf of Mexico, which was later mapped by the USGS (Reference 2.4.6-217). Known as the East Breaks slump, the site is over 1000 km (620 mi.) from the LNP site, and is marked by a 20 km (12.4 mi.) indentation in the shelf edge (Reference 2.4.6-217). Beryhill et al. estimated that the slump occurred 5000 to 10,000 years ago (Reference 2.4.6-217); however, McGregor suggests that it may have occurred as long ago as 15,000 to 20,000 years (References 2.4.6-218 and 2.4.6-219). The total estimated volume of the slide is 50 to 60 cubic kilometers (km^3) (12 to 14.4 cubic miles [$mi.^3$]), and the slump deposits cover more than 3200 km^2 (1200 $mi.^2$) (Reference 2.4.6-217).

A recent study conducted by the USGS (Reference 2.4.6-214) summarized the threat of landslides in the Gulf of Mexico as follows (Figure 2.4.6-206):

> Landslides in the Gulf of Mexico occur in all three depositional provinces (carbonate, salt, and canyon/fan). The largest failures are found in the canyon/fan province. . . . Available information suggests they occurred during the early part of the Holocene (10,000 - 15,000 yr BP). The resumption of hemipelagic sedimentation in the head of Mississippi Canyon at 7500 yr BP indicates that at least the largest of these landslide complexes had ceased being active by mid-Holocene time.
>
> Landslides within the salt province are in general considerably smaller than those in the canyon/fan province, many of them are confined to the walls of mini-basins, but some occupy the Sigsbee escarpment. These landslides appear to be active and are driven by salt creep. Landslides in the carbonate provinces that fringe the eastern and southern Gulf of Mexico appear to have been derived from both the steep West Florida and Campeche Escarpments as well as from the gentler slope above the escarpments. The northern part of the Florida Escarpment has probably undergone little erosion since it originally formed during the Cretaceous, but the southern part of the Florida Escarpment shows sign of active erosion.

2.4.6.4 Propagation of Tsunami Waves

2.4.6.4.1 Propagation in Deep Waters

Tsunami waves travel on the surface of the ocean outward and away from the source in all directions (Reference 2.4.6-205). A tsunami is composed of a series of large amplitude, shallow-water (wavelength, $\lambda > 20\ H$, where H is water depth) gravity waves. Even when generated in deep water, tsunamis are considered shallow-water waves because typical wavelengths can exceed 200 km (120 mi.), while ocean depths are only a few kilometers. The depth of the Caribbean Sea, for example, is 2.6 km (1.6 mi.) (Reference 2.4.6-224). Tsunami waves are generally long, though the actual wavelength and period of tsunami waves are dependent on the source mechanism and its characteristics. For example, tsunamis originating from a large earthquake over a large area will have a much larger initial

wavelength and period than a tsunami generated by a local landslide. Tsunami wave crests can span lengths up to 1000 km (621.4 mi.). The period of tsunami waves typically ranges from 5 to 90 minutes. The height of a tsunami wave on the deep ocean will depend on its source, but it will generally be anywhere from a few centimeters to a meter or more (Reference 2.4.6-205).

When a tsunami is produced, its energy is distributed throughout the water column, regardless of the ocean's depth. In fact, tsunami waves in the deep ocean can travel at high speeds over large distances and lengths of time without losing much energy (Reference 2.4.6-205). According to the USGS (Reference 2.4.6-224), "Tsunamis propagate at the shallow water gravity wave phase speed of $c = (gH)^{1/2}$, which can be in excess of 222 m/s (~ 800 [kilometers per hour] km/hr) [500 miles per hour {mph}], until they dissipate or encounter a shelf and shallow coastal water where they slow to 8 to 14 m/s (~30 to 50 km/hr) [19 to 31 mph]". This indicates that tsunamis travel fastest in deep waters. At the deepest ocean depths, a tsunami wave can travel at 800 km/h (497.1 mph), which is comparable to the speed of a jet aircraft (Reference 2.4.6-205).

2.4.6.4.2 Propagation in Shallow Waters

When tsunamis enter shallow waters typically found at coastlines, bays, or harbors, their speed decreases to 50 to 60 km/h (31 to 37 mph). At the same time, waves farther from shore and in deeper waters are traveling toward the same area at much greater speeds. The waves are compressed in the shallow water such that the wavelength is shortened. Because the wave energy is then applied over a smaller volume of water and the wave energy is directed upward, the waves grow in height. Tsunamis generally arrive on shore with a wavelength exceeding 10 km (6.2 mi.), and successive wave crests arrive anywhere from 10 to 45 minutes apart. However, the flooding from a single wave can last from 10 minutes to 30 minutes, such that the period of danger during a tsunami event might exceed several hours (Reference 2.4.6-205).

Features such as water depth and coastal configuration may cause a significant amount of wave refraction, which can also serve to converge energy and increase wave heights. In addition, a tsunami that occurs during high tide or a localized storm will produce cumulative effects resulting in an even more severe event. A 1-m (3.28-ft.) tsunami in the deep ocean may transform into a 30 to 35 m (98 to 115 ft.) wave onshore. Such waves can cause extensive damage to life and property (Reference 2.4.6-205).

2.4.6.5 Analysis of Historical Tsunami Events

Any of the world's oceans, inland seas, and large bodies of water may experience a tsunami event. The majority of the tsunamis occur in the Pacific Ocean as a result of its large size (more than one-third of the Earth's surface) and the presence of highly active seismic regions. Less common, destructive tsunamis have also originated in the Atlantic and Indian oceans, in the Mediterranean Sea, and within smaller bodies of water, such as the Caribbean Sea. According to the International Tsunami Information Center, "In the last decade alone, destructive tsunamis have occurred in Nicaragua (1992), Indonesia (1992, 1994, 1996), Japan (1993), Philippines (1994), Mexico (1995), Peru (1996, 2001), Papua-New Guinea (1998), Turkey (1999), and Vanuatu (1999)" (Reference 2.4.6-205).

However, according to NOAA's NGDC, only a small percentage of all tsunami events are destructive (Figure 2.4.6-207) (Reference 2.4.6-220). In the past 500 years, 100 tsunamis have been reported in the Caribbean region, only 30 of which caused significant damage (Reference 2.4.6-207). Many of these events were the result of large shallow earthquakes in the Caribbean (Reference 2.4.6-209). Not all earthquakes generate tsunamis, but thrust, reverse, or normal faulting earthquakes of magnitude, $M_W \geq 6.5$, which deform or rupture the seafloor are the most likely to produce tsunamis (Reference 2.4.6-215). The Richter magnitude of an earthquake must generally exceed $M_L = 7.5$ if it is to produce a destructive tsunami. Considering all source mechanisms, the most destructive tsunamis are the result of large, shallow earthquakes with an epicenter or fault line near the ocean floor. Such events are common in highly seismic regions characterized by the collision of tectonic plates, and in particular, by tectonic subduction (Reference 2.4.6-205).

2.4.6.5.1 Historical Tsunamis Generated in the Caribbean

The North Panama Deformation Belt (9-12 degrees [°]N, 83°W-77°W) and the Northern South America Convergence Zone (11.5°-14°N, 77°W-64°W) lie in the southern portion of the Caribbean region (Figure 2.4.6-208) (Reference 2.4.6-214). The North Panama Deformation Belt has a relatively slow rate of convergence (~7-11 millimeter per year [mm/yr]), resulting in a long recurrence interval for large earthquakes (Reference 2.4.6-214). However, in 1882 the source produced an $M_W = 8.0$ event known as the 1882 Panama Earthquake (Figure 2.4.6-209). Despite significant local tsunami damage, there is no report of a tsunami impacting the Gulf Coast as a result of this earthquake (Reference 2.4.6-214). In a thorough review of the seismic threats in the southern Caribbean (Figure 2.4.6-210), the USGS concluded that sources in this region, "...do not appear to be capable of generating very large earthquakes, and thus do not appear to pose a significant tsunami hazard to the Gulf of Mexico coastal zones" (Reference 2.4.6-214).

The Puerto Rico Trench and Hispaniola Trench both lie in the northern portion of the Caribbean region. Though there is no historical record of large earthquakes originating from the Puerto Rico Trench (Figure 2.4.6-211), it is a potentially tsunamigenic seismic source. The largest instrumentally recorded event occurred in 1943 and was an $M_W = 7.3$ earthquake, though McCann suggests that a 1787 earthquake north of Puerto Rico had a magnitude, $M_W = 8.0$ (Reference 2.4.6-214). The Hispaniola Trench (Figure 2.4.6-212) also poses a tsunamigenic threat. In fact, relatively larger earthquakes and more vertical motion are expected for the Hispaniola Trench than for the Puerto Rico Trench (Reference 2.4.6-214). Several earthquakes of magnitude $M_S = 7.0$ to 8.1 (M_W 6.8 to 7.6) occurred between 1946 and 1953 in northern Hispaniola. A destructive local tsunami was produced by one of the 1946 earthquakes (Reference 2.4.6-214).

McCann (Reference 2.4.6-221) examined the seismic reflection records of Western Puerto Rico to characterize tsunamigenic faults that may have a potential to generate tsunamic hazards. He found that the Mona Passage, which is a segment of island arc crust lying between the islands of Puerto Rico and Hispaniola, has many active faults as a result of rapid extension. While some of these active faults are capable of producing earthquakes as large as magnitude $M_W = 7$, most are relatively short in length and are probably only capable of producing events in the magnitude $M_W = 6$ ranges. However, of the 84 active faults, 30 should be considered potentially tsunamigenic, as they are considered capable of producing events of magnitude $M_W = 6.5$ or larger (Reference 2.4.6-221).

According to the USGS (Reference 2.4.6-214),

> The northern Caribbean subduction zone has the potential to cause a major tsunami similar to the 2004 Sumatra tsunami. However, detailed work in the Puerto Rico Trench indicates that slip there is highly oblique and the subducting lithosphere is very old, two indications that perhaps the subduction zone is not capable of generating very large earthquakes. The Hispaniola segment of this subduction zone, while perhaps capable of very large earthquakes, is fringed to the north by an almost continuous line of islands and shallow banks that obstruct, but not completely block, propagating tsunami waves.

It is believed that major earthquakes produce many underwater landslides. However, the energy of tsunamis generated by submarine landslides and slumps is thought to dissipate rapidly as the waves travel across the ocean or even within partially enclosed water bodies such as lakes and fjords (Reference 2.4.6-205). Due to their steep slopes and shallow waters, many islands in the Caribbean region are prone to landslides and slumps (Reference 2.4.6-215). Such an event likely occurred just north of Puerto Rico, and may have been the result of ongoing plate-tectonic movement that tilted the seafloor 4° down to the north. This tilt may have caused massive slope failures that are continuing, as evidenced by large fissures in the seafloor (Figure 2.4.6-204) (Reference 2.4.6-207).

2.4.6.5.2 Historical Tsunamis Generated in the Gulf of Mexico

In contrast to the Caribbean, the Gulf of Mexico contains no subduction zone faults that are a primary source of large, tsunamigenic earthquakes (Reference 2.4.6-214). The Gulf of Mexico has produced some notable earthquakes in the recent past. The most recent and largest event occurred in September of 2006 and had a magnitude of $M_W = 5.8$. However, most of these events have been produced at locations distant from faults and plate boundaries, and are generally known as "midplate" earthquakes. These events result from the release of long-term tectonic stresses that originated from forces applied at the plate boundary, and they are generally rare. With regard to the most recent and largest seismic event in the Gulf, the USGS National Earthquake Information Center suggests that, "Earthquakes of this magnitude are unlikely to generate destructive tsunami. No significant tsunami was generated by this earthquake" (Reference 2.4.6-216). Given the infrequent occurrence and modest magnitude of "midplate" seismic events, there is little likelihood that a seismic event in the Gulf of Mexico would produce a tsunami.

Though the Gulf of Mexico is also characterized by frequent translational landslides, no tsunamis originating from this source have been documented instrumentally or in the geologic record for the Gulf Coast (Reference 2.4.6-206). Trabant et al. (Reference 2.4.6-217) performed a preliminary calculation to estimate the offshore wave-height of the tsunami associated with the historic East Breaks slump at 7.6 m (25 ft.). It should be noted that this calculation has not been supported by subsequent publication, and there is no documented geologic evidence of the impact of such a wave along the Gulf Coast.

The closest volcanoes to the LNP site are located in the southwestern region of the Gulf of Mexico (Figure 2.4.6-201) (Reference 2.4.6-207) and are also abundant in the eastern

Caribbean Sea among the Lesser Antilles. However, no tsunamis as a result of recent volcanic eruptions or associated mass wasting events have been documented in the Gulf of Mexico (Reference 2.4.6-206).

2.4.6.5.3 Historical Tsunamis Generated from Sources Situated Other than the Gulf of Mexico and Caribbean

Potential far-field tsunamigenic sources include the Aleutian Trench in Alaska, the Azores - Gibraltar fracture zone (near Lisbon, Portugal), and far-field submarine landslides. As previously discussed, the impact of the tsunami generated by the 1964 Alaska earthquake was less than 1 m (3.28 ft.) in the Gulf of Mexico. The potential threat of the Azores - Gibraltar fraction zone as a tsunamigenic source is discussed in FSAR Subsection 2.4.6.6.1.

In a report to the NRC (Reference 2.4.6-214), the USGS summarizes the tsunamigenic threat of far-field submarine landslides to the Gulf and Atlantic Coasts as follows:

> Far-field submarine landslide sources have been quoted as potential sources for trans-oceanic tsunamis. The most widely known is the threat of a large-volume landslide caused by an imminent eruption of Cumbre Vieja volcano in the Canary Island. However, models of tsunami propagation, which take into account dispersion and nonlinearity of the landslide-generated waves, show rapid amplitude decay with distance and predict <1 meter of flooding in Florida. In addition, the recurrence time of a major eruption-related landslide is 10^5 yr. The giant Storegga landslide offshore Norway caused large tsunami waves within 600 km radius in the northeast Atlantic, but the waves are not known to have propagated to the U.S. East Coast. Some large landslides have been identified along the Scotian margin north off New England. Most of them are Holocene and older in age and appear to be related to the expansion and contraction of the Laurentide ice sheet. The 1929 Grand Banks landslide generated a damaging tsunami locally, but not in New England. However, larger landslides than the 1929 Grand Banks landslide have been identified in the stratigraphic record.

Impulsive events such as meteor and asteroid strikes and nuclear explosions are unlikely, but are potential near-field and far-field tsunamigenic sources.

2.4.6.6 Tsunami Water Levels

2.4.6.6.1 Water Levels Due to Simulated Historic Earthquakes

In addition to the recorded events in the Gulf of Mexico, numerical simulations of tsunamis generated by historic earthquakes provide additional insight into the potential tsunami hazards in the Gulf of Mexico. Wave generation and propagation modeling of the tsunami generated by the 1755 Lisbon (M_w = 8.7) earthquake was conducted using the nonlinear long wave equations and a 10-minute Mercator grid for the Atlantic Ocean (Figure 2.4.6-212). The modeling predicted a teletsunami (i.e., a tsunami from a source over 1000 km [621.4 mi.] away) arriving in the Caribbean and entering the Gulf of Mexico (Reference 2.4.6-213). Mader states:

> ...the east coast of the U.S.A. and the Caribbean [would] receive a tsunami wave offshore in deep water about two meters [6.6 feet] high with periods of 1.25 to 1.5 hours. Such a wave would give waves along the shore about 10 feet [3.0 meters] high with Saba being unique with about a 20 feet [6.1 meters] high wave after run-up. After the wave travels into the Gulf of Mexico the wave amplitudes are less than one meter (Reference 2.4.6-213).

2.4.6.6.2 Water Levels Due to Simulated Potential Tsunamigenic Seismic Events Identified by NOAA

The NOAA West Coast and Alaska Tsunami Warning Center has identified four seismic tsunamigenic sources that could potentially produce "worst-case" impacts for the Gulf Coast. These locations were selected based on the results of numerical models that simulated hypothetical tsunamis originating in the Atlantic Ocean, Gulf of Mexico, and Caribbean Sea (Reference 2.4.6-225). The four sources are shown on Figure 2.4.6-213. The point of origin and magnitude of the four earthquakes are as follows: 1) the Puerto Rico Trench (66°W, 18°N, M_w = 9.0); 2) the Caribbean Sea (85°W, 21°N, M_w = 8.2) from the Swan fault to the mouth of the Gulf of Mexico near Cancun; 3) the North Panama Deformed Belt (66°W, 12°N, M_w = 9.0); and 4) the Gulf of Mexico off the coast of Veracruz, Mexico (95°W, 20°N, M_w = 8.2) (Reference 2.4.6-225).

According to Knight (Reference 2.4.6-225), a simulated tsunami generated by a seismic event (M_w = 9.0) in the Puerto Rico Trench (Figure 2.4.6-214) has unique impacts on the Gulf and Atlantic coasts, respectively. The tsunami resulting from the specified seismic event impacts the Atlantic Coast with an amplitude exceeding 150 centimeters (cm) (59 inches [in.]), and with a leading edge elevation. In contrast, the tsunami waves impacting the Gulf Coast as a result of the same event have much lower amplitudes (less than 25 cm [9.8 in.]), and are characterized by a leading edge depression (Figure 2.4.6-215) (Reference 2.4.6-225).

For a tsunami generated outside of the Gulf of Mexico to impact lands in the Gulf, such as from the Puerto Rico Trench source, it must travel through either the Caribbean Sea or the Straits of Florida. According to Knight's analysis using Kowalick and Murty's energy flux vector,

$$\rho d\vec{V}\left(g\zeta + \frac{1}{2}V^2\right), \qquad \text{Equation 2.4.6-1}$$

the path via the Caribbean is 1 hour faster, but more energy reaches the Gulf of Mexico via the Straits of Florida than via the Caribbean pathway (Reference 2.4.6-225). A separate analysis of energy losses due to friction suggests that significant energy losses occur in the Caribbean region due to bottom friction (Figure 2.4.6-216). A dissipation curve representing these energy losses due to bottom friction is shown on Figure 2.4.6-217.

Knight's analysis also suggests that roughly 10 times more energy flows into the Atlantic Ocean than into the Caribbean as a result of the tsunami originating at the Puerto Rico Trench (Reference 2.4.6-225). This is supported by work presented by Maul, as shown on

Figure 2.4.6-218 (Reference 2.4.6-226). A summary of the peak wave elevations generated by a tsunami originating at the Puerto Rico Trench is shown in Table 2.4.6-204. The resulting wave amplitudes at Gulf Coast locations are 25 cm (10 in.) or less (Reference 2.4.6-225).

Similar analyses were performed for the remaining three sources indicated by NOAA to be capable of generating "worse-case" events. The initial amplitudes of a tsunami generated by a seismic event (M_w = 8.2) in the Caribbean Sea near Cancun are shown on Figure 2.4.6-219. The resulting tsunami amplitude is less than 30 cm (12 in.) in the Gulf Coast, again as a result of significant energy losses due to bottom friction in the Caribbean Sea (Reference 2.4.6-225).

The initial amplitudes of a tsunami generated by a seismic event (M_w = 9.0) near Venezuela are shown on Figure 2.4.6-220. In this case, Gulf Coast impacts are mitigated due to energy losses via bottom friction, and over time, as a result of multiple wave reflections in the Caribbean Sea. The resulting maximum tsunami waves in the Gulf Coast are less than 15 cm (5.9 in.), while Atlantic Coast waves are under 50 cm (20 in.) (Reference 2.4.6-225).

The NOAA West Coast and Alaska Tsunami Warning Center suggests that sources outside of the Gulf of Mexico will not likely produce a tsunami capable of damaging the Gulf Coast. There are only two paths available to a tsunami originating outside of the Gulf of Mexico — through the narrow Straits of Florida and through the Caribbean. In both cases, the tsunami's energy losses due to bottom friction would be significant. As a result, the Gulf Coast is effectively shielded from sources outside of the Gulf of Mexico (Reference 2.4.6-225).

The scenario of an earthquake in the Gulf of Mexico off the coast of Veracruz, Mexico, is based on a hypothetical scenario. This region has been seismically active historically. The initial amplitudes of a tsunami generated by a seismic event (M_w = 8.2) in the Gulf of Mexico near Veracruz are shown on Figure 2.4.6-221. Most of the energy produced in this event is confined to the Gulf of Mexico. The resulting tsunami impacting the Gulf Coast would have amplitudes less than 35 cm (14 in.) (Reference 2.4.6-225).

In 2007, the USGS conducted a preliminary analysis (Reference 2.4.6-214) of tsunami threats to the United States Gulf and Atlantic coasts as a compliment to Knight's study (Reference 2.4.6-225). The USGS evaluated the tsunami threat of the following five seismic sources in the Caribbean: 1) the west Cayman oceanic transform fault (OTF), also known as Swan Island fault; 2) the east Cayman (OTF), also known as Oriente fault; 3) the northern Puerto Rico/Lesser Antilles subduction zone (SUB); 4) the north Panama deformation belt, classified by Bird (Reference 2.4.6-227) as an oceanic convergent boundary (OCB); and 5) the north coast of South America convergence zone classified by Bird (Reference 2.4.6-227) as a subduction zone (SUB) (termed the north Venezuela subduction zone below) (Reference 2.4.6-214). A classification scheme by Bird (Reference 2.4.6-227) was used to determine the most likely maximum rupture length and earthquake magnitude associated with each of the sources (Reference 2.4.6-214). The range of magnitude and average slip for each fault source are presented in Table 2.4.6-205.

In the USGS study, "Tsunami propagation was modeled using the linear long-wave equation, numerically implemented with a leap-frog, finite-difference algorithm." Because

linear theory is most readily applied to deep-ocean tsunami propagation, the model was limited to a depth of 250 m (820.2 ft.), such that propagation across the continental shelf and wave runup were not modeled. However, the study suggests that runup can be approximated as 3 times the tsunami amplitude at a water depth of 250 m (820.2 ft.), accounting for shoaling and runup amplification. This approximation does not include energy dissipation from geometric spreading, bottom friction, and nonlinear attenuation. The model's spatial grid size is 2 arc-minutes. Tsunami propagation was modeled using an 8-second time step, for a total simulation time of 4.4 to 6.6 hours (Reference 2.4.6-214).

The simulation results for each source are presented on Figures 2.4.6-222, 2.4.6-223, 2.4.6-224, 2.4.6-225, and 2.4.6-226, which show the maximum open ocean tsunami amplitude out of 100 simulations for each source. The results suggest that the transform faults (OTF) are much less efficient at generating tsunami waves (Figures 2.4.6-222 and 2.4.6-223) than the thrust faults along subduction zones (SUB) and oceanic convergent boundaries (OCB) (Figures 2.4.6-224, 2.4.6-225, and 2.4.6-226) (Reference 2.4.6-214). In general, within the Gulf of Mexico tsunami amplitudes are highest "where the shelf edge is approximately normal to the incidence of tsunami waves propagating from the south (i.e., between ~83-85°W and ~87.5-88.5°W)". A time series analysis indicates that, with the exception of the northern Puerto Rico subduction zone scenario, tsunami onset is "emergent" in the Gulf of Mexico, such that initial tsunami waves are smaller than some of those that come after. This is due, in part, to the natural obstructions to the wave propagation (Reference 2.4.6-214).

Figure 2.4.6-227 shows the range of peak offshore tsunami amplitudes from all 100 simulations at the 250-m (820.2-ft.) isobath for a latitudinal profile in the Gulf of Mexico. The maximum tsunami wave height is roughly 0.65 m (2.1 ft.), and is generated by the Venezuela subduction zone scenario (Reference 2.4.6-214). Though impacts will vary because of nearshore propagation and runup effects, we can estimate the maximum runup height at 2.0 m (6.6 ft.) (3 x 0.65 m = 1.95 m ~ 2.0 m). The maximum tsunami wave height generated by the other four sources is less than 0.25 m (10 in.), suggesting a maximum runup height of less than 0.75 m (2.5 ft.).

The simulation results indicate that the most severe impacts for the Gulf Coast are the result of large earthquakes along the north Venezuela subduction zone. However, it should be noted that the resulting tsunami amplitudes were heavily dependent on the seismic event magnitude for each source. The USGS (Reference 2.4.6-214) summarizes its findings as follows:

> In general, these results are consistent with the findings of Knight (2006) [Reference 2.4.6-225], where the far-field tsunamis generated from earthquakes located beneath the Caribbean Sea are higher along the Gulf coast than the Atlantic coast because of dissipation through the Greater Antilles islands. Conversely, tsunamis generated from earthquakes north of the Greater Antilles are higher along the Atlantic coast than the Gulf coast.

The USGS study concludes by suggesting that more refined hydrodynamic modeling is needed in order to determine the potential tsunami impact on the Gulf Coast due to tsunami events generated by the seismic sources in the Caribbean (Reference 2.4.6-220).

2.4.6.6.3 *Water Levels Due to Worst Case Tsunamigenic Events Using a Simplified Formula-Based Approach*

A simplified formula-based approach of tsunami analysis was derived from many computer simulations of tsunamis based on the linear dispersive water wave theory (Reference 2.4.6-229). The application of the tsunami simulation approach to earthquake and landslide tsunamis have been thoroughly presented by Ward (Reference 2.4.6-232), Ward and Asphaug (Reference 2.4.6-233), and Ward and Day (Reference 2.4.6-234). This approach is mode and ray-based and includes landslide evolution, geometrical spreading, dispersive spreading, frequency dependent shoaling, and diffractive corrections. Like many tsunami simulations, this approach takes the waves to a shallow water location near the site of interest.

The formula-based approach does not require detailed computer modeling and it makes many simplifications compared with the simulation-based approach (Reference 2.4.6-230). Due to these simplifications, the formula-based approach overestimates the magnitude of wave runup in many situations. In addition, the formula-based approach attempts to embody the same processes (generation, spreading, shoaling, runup) as the simulation-based approach but uses simplified approximations of the processes instead of more rigorous computer calculations.

Certain parameters in the formula-based approach were obtained by fitting output created by many runs from a full simulator; in this sense, the formula- and simulation-based approaches are linked. In general, according to the formula-based approach, the wave runup η can be represented as a product of the following components:

$$\eta = A_0 PSB \qquad \text{Equation 2.4.6-2}$$

where A_0 is the source amplitude, P is the propagation loss (less than 1.0), S is the shoaling correction (usually more than 1.0), and B is the amplification due to beaching. The procedure to calculate these components is explained below.

2.4.6.6.3.1 Determination of Source Amplitude A_0

In the case of a landslide, A_0 is given as:

$$A_0 = 3.5T\left(\frac{V_s}{\sqrt{gH_0}}\right)^{1.8} \qquad \text{Equation 2.4.6-3}$$

where T is the thickness of the landslide unit, V_s is the landslide speed, g = 9.8 m/s^2 (32.2 ft/s^2), and H_0 is the water depth at the slide. Faster moving slides tend to produce bigger waves. Equation 2.4.6-3 is applicable for all landslide velocities satisfying $0<V_s<\sqrt{gH_0}$. Whereas, the initial tsunami amplitude approximated by Silver et al. (Reference 2.4.6-230) is:

$$A_0 = T \qquad \text{Equation 2.4.6-4}$$

It is clear from these two expressions (Equations 2.4.6-3 and 2.4.6-4) that, for the initial tsunami amplitude, Equation 2.4.6-3 is more complicated than Equation 2.4.6-4 (Reference 2.4.6-230), as the former tries to account for the effect of landslide velocity whereas the latter does not. Equation 2.4.6-3 was derived by fitting the results from many numerical landslide tsunami experiments in Ward's equation (Reference 2.4.6-236). It can be noted that for nominal landslide speeds (V_s~$0.5\sqrt{gH_0}$), both approximations (Equations 2.4.6-3 and 2.4.6-4) for the initial tsunami amplitude give nearly equal results. The range of V_s values used in Equation 2.4.6-3 can be estimated from the "terminal velocity" of low basal friction slides $V_{term} = \sqrt{\frac{g \sin \Theta}{Cd}}$ where Θ is slope of the surface, and Cd the coefficient of dynamic friction. For underwater landslides, Ward and Day (References 2.4.6-238 and 2.4.6-239) used values Cd = (2 to 20)x10^{-4}/m ([6.6 to 66]x10^{-4}/ft.). Regardless of the value of Cd selected, the important feature is that the plausible range of V_s used in Equation 2.4.6-3 be lower for slides on shallow slopes and larger for slides on steep slopes.

In case of an earthquake, A_0 is given as:

$$A_0 = \alpha \Delta u. \qquad \text{Equation 2.4.6-5}$$

where Δu is earthquake slip and α is a fraction of slip that transforms into uplift. This factor depends upon the style of the fault. Mathematically, α can be determined using the following relationship:

$$\alpha = (1 - \phi/180) Sin(\phi) Sin(\rho) \qquad \text{Equation 2.4.6-6}$$

where ϕ and ρ are the dip and rake angles, respectively, in degrees. Combining Equations 2.4.6-5 and 2.4.6-6, A_0 for an earthquake is given as:

$$A_0 = (1 - \phi/180) Sin(\phi) Sin(\rho) \Delta u \qquad \text{Equation 2.4.6-7}$$

The most efficient mechanism for tsunami generation have ϕ near 45 degrees and ρ = ± 90 degrees. Our test quakes employed these values.

2.4.6.6.3.2 Determination of Propagation Loss P

Propagating tsunami waves go through significant transformations such as modification in wave shape, duration, and attenuation in amplitude. The attenuation in tsunami wave amplitude is roughly proportional to inverse distance traveled due to geometrical spreading and frequency dispersion (Reference 2.4.6-228). For a constant depth ocean, Ward and Asphaug (Reference 2.4.6-233) fit the peak tsunami amplitude by the following relationship:

$$P = \left(1 + \frac{2R}{D}\right)^{-\varphi} \qquad \text{Equation 2.4.6-8}$$

where R is the distance of measurement point from the source, D is the dimension of the tsunami source, and φ is an exponent defined as

$$\varphi = 0.5 + 0.575\exp\left(-0.0175\frac{D}{H_0}\right)$$ Equation 2.4.6-9

The first term in Equation 2.4.6-9 accounts for geometrical spreading. The second term in Equation 2.4.6-9 accounts for additional wave height losses due to frequency dispersion. Generally larger dimensioned sources decay slower with distance on this account. Typically the value of φ from Equation 2.4.6-9 varies between 0.7 and 1.0. Combining Equations 2.4.6-7, 2.4.6-8, and 2.4.6-9, the peak wave amplitude at a distance R from the source A(R) can be determined by the following equations:

For Earthquake:

$$A(R) = A_0 P = \left(1 - \frac{\phi}{180}\right) Sin(\phi) \left| Sin(\rho) \right| \Delta u \left(1 + \frac{2R}{D}\right)^{-\left[0.5 + 0.575\exp\left(-0.0175\frac{D}{H_0}\right)\right]}$$

Equation 2.4.6-10

For Landslide:

$$A(R) = A_0 P = 3.5T \left(\frac{V_s}{\sqrt{gH_0}}\right)^{1.8} \left(1 + \frac{2R}{D}\right)^{-\left[0.5 + 0.575\exp\left(-0.0175\frac{D}{H_0}\right)\right]}$$

Equation 2.4.6-11

2.4.6.6.3.3 Determination of Shoaling Correction S

Equation 2.4.6-8, which led to Equations 2.4.6-10 and 2.4.6-11, assumes oceans of constant depth H_0. Toward shore, however, real oceans become shallow to depth H_S. When tsunamis reach shallow water, they slow and grow to conserve energy flux. For the waves of interest, deep water amplitude A(R) given by Equations 2.4.6-10 and 2.4.6-11 needs to be corrected to account for shoaling. According to linear theory, the shoaling correction, S, is given by the following relationship (Reference 2.4.6-228):

$$S = \left[\frac{V_G(\omega_{\max}, H_0)}{V_G(\omega_{\max}, H_S)}\right]^{\frac{1}{2}}$$ Equation 2.4.6-12

where $V_G(\omega_{\max}, H_0)$ and $V_G(\omega_{\max}, H_S)$ are the tsunami wave group velocities at ocean depths H_0 and H_S, respectively. It is clear from Equation 2.4.6-12 that the shoaling amplification depends on the ratio of group velocity at the source site and the coast site evaluated at the frequency associated with the peak tsunami height. As we are interested in a simplified formula versus full simulation, Equation 2.4.6-12 can be approximated using a long wave assumption (Reference 2.4.6-228) as:

$$S = \left(\frac{H_0}{H_S}\right)^{\frac{1}{4}}$$ Equation 2.4.6-13

Using Equation 2.4.6-13, the shoaled amplitude A(S) is defined as a function of the peak wave amplitude A(R) at distance R from the source as:

$$A(S) = A(R)\left(\frac{H_0}{H_S}\right)^{\frac{1}{4}}$$ Equation 2.4.6-14

2.4.6.6.3.4 Applying Beaching Correction

Runup height η_{est} is estimated using the following empirical formula (Reference 2.4.6-228):

$$\eta_{est} = A(S)^{4/5} H_S^{1/5}$$ Equation 2.4.6-15

Using Equation 2.4.6-15, one can estimate wave runup from offshore shoaled wave height. Combining Equations 2.4.6-14 and 2.4.6-15, the estimated runup can be calculated using the following relationship:

$$\eta_{est} = A(R)^{4/5} H_0^{1/5}$$ Equation 2.4.6-16

Using Equation 2.4.6-16, one can estimate runup using offshore wave height A(R) and source water depth H_0. In order to be clear in terminology, the following terms are defined:

Runup height, η, is the maximum elevation that a tsunami reaches. Runup height can be either an actual observed value η_{obs} or an estimated value η_{est}.

Run-in distance, X, is the maximum distance inland that a tsunami reaches. Run-in distance can be either an actual observed value X_{obs} or an estimated value X_{est}. The topographic elevation at the run-in distance X_{obs} equals the runup height η_{obs}.

Flow Depth, $F_d(X)$, is the depth of the flowing water at various places X onshore. Flow depth goes from its maximum value $F_d(0)$ at the shoreline to $F_d(X_{obs})$ = 0 at the run-in distance X_{obs}.

2.4.6.6.3.5 Determination of Run-in Distance

Hills and Mader (References 2.4.6-231 and 2.4.6-240) estimated run-in distance as:

$$X_{est} = 0.06 F_d(0)^{1.33} n^{-2}$$ Equation 2.4.6-17

where X_{est} is the estimated run-in distance in meters, $F_d(0)$ is the flow depth at the shoreline in meters, and n is Manning's roughness coefficient. This equation was modified by McSaveney and Rattenbury (Reference 2.4.6-240) to include a slope factor:

$$\frac{dF_d(X)}{dX} = -\left[\frac{16.7n^2}{F_d(0)^{0.33}} + 5Sin(\theta)\right] \qquad \text{Equation 2.4.6-18}$$

where $dF_d(X)/dX$ is the loss in flow depth per meter of run-in distance and θ is the beach slope. Integrating Equation 2.4.6-18 provides:

$$F_d(X) = F_d(0) - \left[\frac{16.7n^2}{F_d(0)^{0.33}} + 5Sin(\theta)\right]X \qquad \text{Equation 2.4.6-19}$$

The maximum run-in distance can be estimated from Equation 2.4.6-19 by substituting $F_d(X)$= 0, as:

$$X_{est} = \frac{F_d(0)^{1.33}}{16.7n^2 + 5F_d(0)^{0.33}Sin(\theta)} \qquad \text{Equation 2.4.6-20}$$

Flow depths are difficult to measure after a tsunami event has occurred. In order to determine actual flow depths, water marks need to be measured on surviving telephone poles, posts, trees, or buildings. Generally on open beaches, these features do not exist and hence flow depth information is not readily available. Moreover, to use Equation 2.4.6-20, flow depth at the shoreline must be known. For applications here, the estimated runup height, η_{est}, from Equation 2.4.6-16 is substituted for flow depth at the shoreline, $F_d(0)$, in Equation 2.4.6-20 to get the following result:

$$X_{est} = \frac{\eta_{est}^{1.33}}{16.7n^2 + 5\eta_{est}^{0.33}Sin(\theta)} \qquad \text{Equation 2.4.6-21}$$

In most cases the estimated runup height, η_{est}, is larger than $F_d(0)$, so the substitution $F_d(0) = \eta_{est}$ in Equation 2.4.6-21 is conservative.

2.4.6.6.3.6 Determination of Tsunami Hazard

Consider a facility located at elevation E_{site} and distance D_{site} from the coast. For the facility to be located in an estimated tsunami hazard zone, the following two conditions must be met:

- Condition 1: The site must have an elevation less than the estimated tsunami runup, η_{est}, ($E_{Site} < \eta_{est}$).
- Condition 2: The site must be closer to the beach than the estimated run-in distance, X_{est}, ($D_{Site} < X_{est}$).

Both of the above conditions ($E_{Site} < \eta_{est}$ and $D_{Site} < X_{est}$) must be satisfied for the site to be considered within the estimated tsunami hazard zone. If one of the conditions is not met, then the site is considered outside of the estimated tsunami hazard zone.

2.4.6.6.3.7 Water Levels at the LNP Site Due to the Worst Case Submarine Landslides in the Gulf of Mexico

FSAR Subsection 2.4.6.3.2.2 provides a detailed discussion of the potential tsunami generators in the Gulf of Mexico, including submarine landslides. In order to conduct a tsunami hazard evaluation for the LNP site, a range of worst case potential tsunami generators were considered in the Gulf of Mexico, including the following submarine landslides:

- East Breaks
- Mississippi Canyon Landslide
- Landslides along the Florida Escarpment
- Along the slope above the Florida Escarpment

The geometrical parameters of the potential tsunami generators listed above were taken from the USGS Report to NRC (Reference 2.4.6-212). These landslides were termed the "Maximum Credible Submarine Landslides" in the USGS Report. Landslide speed can strongly affect tsunami size; generally faster moving slides generate larger waves and slower moving slides generate smaller waves (FSAR Subsection 2.4.6.6.3.1). Landslide speed can vary considerably depending upon the properties of the slide material and the slope and distance over which the slide moves. While conducting tsunami hazard evaluation for a given slide, a range of possible slide speeds from 25 to 50 m/s were considered.

Figure 2.4.6-228 (References 2.4.6-212 and 2.4.6-235) indicates that the depth of the slope above the Florida Escarpment ranges from 200 to 1000 m (656.2 to 3280.8 ft.), resulting in an average depth of 600 m (1968.5 ft.). Based upon Figure 2.4.6-229 (Reference 2.4.6-241), the east-west lateral dimension of the West Florida Slope (that is, the slope above the Florida Escarpment) is approximately 50 km (31.1 mi.) from the 200 m (656.2 ft.) water depth shelf break off the west coast of Florida to the 1,500 m (4921.2 ft.) water depth at the top of the Florida Escarpment, resulting in a slope of 1.5 degrees.

Figure 2.4.6-228 (References 2.4.6-212 and 2.4.6-235) indicates that the depth of the top of the Florida Escarpment is between 1500 and 2500 m (4921.2 and 8202.1 ft.), resulting in an average depth of 2000 m (6561.7 ft.). The average gradient of the Florida Escarpment is at least 20 degrees.

As described above, the slope of the slope above the Florida Escarpment is far less than the slope of the Florida Escarpment. As such, it would be expected that the speed of slides on the slope above the Florida Escarpment would be considerably less than the speed of slides on the Florida Escarpment. Based on the description presented in FSAR Subsection 2.4.6.6.3.1, the terminal landslide velocity, V_{term}, is proportional to the square root of sin of gradient as given below:

$$V_{term} \propto \sqrt{\sin \Theta} \qquad \text{Equation 2.4.6-22}$$

Using Equation 2.4.6-22, a relationship can be established between landslide velocities of the slope above the Florida Escarpment and the Florida Escarpment as given below:

$$\frac{V_{term}(Slope)}{V_{term}(Escarpment)} = \sqrt{\frac{\sin\Theta_{Slope}}{\sin\Theta_{Escarpment}}} \approx 0.28 \qquad \text{Equation 2.4.6-23}$$

If a velocity of 25 to 50 m/s (82 to 164 ft./sec) is used for slides on the Florida Escarpment, then a velocity of 7 to 14 m/s (23 to 45.9 ft./sec) can be estimated for slides on the slope above the Florida Escarpment. Assumption of a larger gradient for the Florida Escarpment results in smaller, less conservative, velocities.

Using the methodology presented in FSAR Subsection 2.4.6.6.3 and landslide input parameters presented in Table 2.4.6-206, landslide analyses were conducted. Table 2.4.6-207 presents impacts of worst case tsunamis at the LNP site generated due to potential submarine landslides in the Gulf of Mexico in terms of runup.

In order to determine run-in distances for various runup values tabulated in Table 2.4.6-207, beach slope and surface roughness are required. The nominal plant grade elevation for the footprints of LNP 1 and LNP 2 is 15.2 m (50 ft.) NAVD88 (FSAR Subsection 2.4.1.1) and the elevation of the Cedar Key datum is 4.06 ft. NAVD88 (Table 2.4.5-204). Further, the coast line of the Gulf of Mexico is about 12.8 km (7.9 mi.) from the LNP site (FSAR Subsection 2.4.1.1). Using this information, the beach slope θ is about 0.06 degree. According to Gerardi et al. (Reference 2.4.6-231), the roughness of the land surface is represented by Manning's coefficient, n, that is 0.015 for smooth topography, 0.03 for urbanized/built land, and 0.07 for densely forested landscape. The landscape between the shoreline and the LNP site falls between urbanized/built land and densely forested category. However, to be conservative, the value of Manning's roughness coefficient, n, was assumed to be 0.03 for the tsunami inundation analysis for the LNP site.

Using the beach slope and surface roughness parameters, run-in distances corresponding to various runup values were determined as tabulated in Table 2.4.6-207.

2.4.6.6.3.8 Water Levels at the LNP Site Due to the Worst Case Earthquake Tsunamis

Using the formula-based approach in FSAR Subsection 2.4.6.6.3, the following worst case earthquake tsunamis were analyzed to determine the flooding impact at the LNP site:

- Mid-Gulf Tsunamigenic Earthquake
- Veracruz Tsunamigenic Earthquake
- Venezuela Tsunamigenic Earthquake

Table 2.4.6-208 presents parameters associated with the worst case earthquakes that were used to determine the impacts of generated tsunamis at the LNP site. Table 2.4.6-209 presents the offshore wave heights, runup heights, and run-in distances corresponding to these earthquake tsunamis.

2.4.6.6.3.9 PMT Water Levels Coincident with Tides, Wind Waves, and Sea Level Anomalies

In FSAR Subsections 2.4.6.6.3.6 and 2.4.6.6.3.7, the runup and run-in values were determined without considering tides, wind waves, sea level anomalies, or the effect of long-term climate change. NRC Regulatory Guide 1.59, however, requires that the 10 percent exceedance astronomical high spring tide be used as the antecedent water level for the storm surge due to a PMH event. The same antecedent water level condition is also used to obtain the PMT maximum water level. The 10 percent exceedance antecedent high spring tide at the Crystal River coastline near the LNP site is taken as 1.3 m (4.3 ft.) MLW, which is equivalent to 0.82 m (2.68 ft.) NAVD88.

As presented in FSAR Subsection 2.4.5.2.2, and according to Regulatory Guide 1.59, the sea level anomaly for Crystal River is 0.18 m (0.6 ft.). Further, the expected sea level rise is 0.12 m (0.39 ft.) for a design period of 60 years for the LNP site.

Combining the 10 percent exceedance high spring tide (2.68 ft. NAVD88), sea level anomaly (0.6 ft.), and the long-term sea level rise (0.39 ft.) with the postulated conservative tsunami runup values at the Florida Gulf Coast shoreline near the LNP site presented in FSAR Subsections 2.4.6.6.3.6 and 2.4.6.6.3.7 results in an increase of 3.67 ft. (1.1 m) NAVD88 (2.68+0.6+0.39 = 3.67 ft.). The associated coincident PMT wave runup and run-in are presented in Tables 2.4.6-210 and 2.4.6-211 for worst case landslides and earthquake tsunamis.

As shown in Tables 2.4.6-210 and 2.4.6-211, the maximum runup height estimates after applying the 10 percent exceedance high spring tide, sea level anomaly, and long-term sea level rise corrections are 22.5 m (73.8 ft) NAVD88 and 6.8 m (22.3 ft) NAVD88 for the worst-case landslide and earthquake, respectively. The corresponding maximum run-in distances are 2.07 km (1.29 mi) and 0.5 km (0.31 mi), respectively. Therefore, the actual runup height will be much smaller than the estimated runup height.

2.4.6.6.3.10 Determination of Tsunami Hazard at the LNP Site

In order to determine whether the LNP site would be impacted by these worst case tsunamis, tsunami hazard criteria described in FSAR Subsection 2.4.6.6.3.6 was used. In Tables 2.4.6-210 and 2.4.6-211, values of η_{est} and X_{est} have been assembled for all plausible scenarios for both cases of with and without tides, wind waves, sea level anomalies, and the effect of longterm climate change for the worst case tsunamis generated by landslides and earthquakes. It is clear that in no case do both conditions ($E_{Site} < \eta_{est}$ and $D_{Site} < X_{est}$) apply to the LNP site. Therefore, tsunamis generated by worst case submarine landslides or earthquakes are not expected to impact the LNP site.

2.4.6.7 Summary and Conclusions

The most common tsunamigenic mechanisms are earthquakes, landslides, and volcanic eruptions. Although meteorites, asteroids, and nuclear explosions are also potential tsunamigenic sources, their occurrence is rare. Based on the literature review of various source mechanisms, the most destructive tsunamis are the result of large, shallow earthquakes with an epicenter or fault line near the ocean floor and a magnitude $M_W \geq 6.5$.

There are no significant near-field tsunamigenic sources threatening the Gulf Coast. The Gulf of Mexico does not have the tectonic conditions that can generate destructive tsunamis. However, the Gulf of Mexico has produced some notable earthquakes in the recent past. The most recent and largest event occurred in September of 2006 and had a magnitude of $M_W = 5.8$. However, given the lack of sliding tectonic plates (subduction of one plate over the other, specifically) and the infrequent occurrence and modest magnitude of these "midplate" earthquakes, there is little likelihood that a seismic event in the Gulf of Mexico would produce a tsunami.

Though the Gulf of Mexico is characterized by frequent landslide events, they have not been a source of any tsunami that has been documented instrumentally or in the geologic record for the Gulf Coast. The potential worst-case scenario may be represented by review of the East Breaks slump — a landslide that likely occurred 5000 to 20,000 years ago. Preliminary analysis of this event suggests that such a landslide would have produced a tsunami with a maximum offshore height of 7.6 m (25 ft.). This calculation has not been supported by subsequent publication, and there is no documented geologic evidence of the impact of such a wave along the Gulf Coast. However, the inland distance and elevation of the LNP site when coupled with the site's distance from the East Breaks slump source suggest that a tsunami with a maximum initial wave height of 7.6 m (25 ft.) would not likely impact the LNP site.

Far-field seismic tsunamigenic sources for the Gulf of Mexico include the Aleutian Trench in Alaska, the Azores - Gibraltar fracture zone, and various locations within the Caribbean Sea. The Caribbean region in particular has several active subduction zones as the result of the movement of the Caribbean plate. Far-field landslides (e.g., the Canary Islands) and volcanoes (e.g., the Lesser Antilles) are also a potential source, but are unlikely to produce tsunamis that will be destructive to the Gulf Coast.

Historical records of tsunami waves along the Gulf Coast indicate an infrequent occurrence and magnitudes too small to cause any significant damage. Three historical tsunami events have been documented for the Gulf Coast in the available tsunami databases and literature. On October 24, 1918, a small wave was recorded at a Galveston, Texas, tide gauge, and was likely generated by an earthquake aftershock originating in the Mona Passage, just northwest of Puerto Rico. On May 2, 1922, a 0.6-m (2-ft.) wave was recorded on a tide gauge in Galveston, Texas, as a result of an earthquake originating near Isla de Vieques, Puerto Rico. Most recently, on March 27, 1964, standing wave activity was recorded throughout the Gulf Coast as a result of an earthquake in Prince William Sound, Alaska. All historical tsunami waves recorded along the Gulf Coast have been less than 1 m (3.28 ft.).

In addition to the recorded events in the Gulf of Mexico, numerical simulations indicate that the 1755 Lisbon earthquake may have also produced a tsunami that impacted the Gulf Coast. If so, the deep-water amplitude of the resulting tsunami would have been reduced to less than 1 m (3.28 ft.) once within the Gulf of Mexico.

NOAA's West Coast and Alaska Tsunami Warning Center evaluated four seismic tsunamigenic sources that could potentially produce "worst-case" impacts for the Gulf Coast. These sources include Puerto Rico Trench, Swan fault, North Panama Deformed Belt, and a hypothetical source just North of Veracruz, Mexico. This study concluded that

sources outside of the Gulf of Mexico will not likely produce a tsunami capable of damaging the Gulf Coast, because bottom friction will result in significant energy losses for a tsunami traveling through the Straits of Florida or the Caribbean Sea. In 2007, the USGS conducted a complimentary study on a similar set of seismic sources within the Caribbean region. The results of this study were limited to deep-water (250 m [820.2 ft.]) amplitudes, but were generally consistent with the NOAA report.

The tsunamigenic threat for the LNP site is negligible. Maximum historic observed tsunami waves have been less than 1 m (3.28 ft.) along the Gulf Coast. No significant near-field threats exist, and the region is effectively shielded from far-field tsunami events by the narrow, shallow waters of the Straits of Florida and Caribbean Sea. Regions of high seismicity in the Caribbean Sea, such as the Puerto Rico Trench, Swan fault, and North Panama Deformed Belt pose the most significant tsunamigenic threat.

Based on runup and run-in calculations due to potential worst case tsunamigenic submarine landslide and earthquake events using the Simplified Formula Approach as described in FSAR Subsection 2.4.6.6.3.10, the LNP site will not be impacted.

2.4.6.8 Hydrography and Harbor or Breakwater Influences on Tsunami

Routing of the controlling tsunami, which includes breaking wave formation, bore formation, and resonance effects, is expected to be minor and limited to shorelines. As the LNP site is approximately 12.8 km (7.9 mi.) from the Gulf of Mexico, hydrography and harbor or breakwater influences are not expected to be severe enough under any circumstances to jeopardize the operation of the safety-related structures.

2.4.6.9 Effects on Safety-Related Facilities

As concluded in FSAR Subsection 2.4.6.7, the LNP site is not expected to be impacted by PMT. Thus, effects of the controlling tsunami are not expected to jeopardize the operation of the safety-related structures. Therefore, measures to protect the LNP site against the effects of a tsunami are not included in the design criteria.

2.4.16 REFERENCES

~~2.4.6-222~~ ~~Zaibo, Narcisse, et al., "Estimation of Far-Field Tsunami Potential for the Caribbean Coast Based on Numerical Simulation," Science of Tsunami Hazards, Volume 21, Number 4, pp. 202 – 222, 2003.~~

~~2.4.6-223~~ ~~"Google Earth," NASA, Europa Technologies, Terremetrics, Tele Atlas, 2007.~~

2.4.6-228 Chesley, S.R., and S.N. Ward, "A Quantitative Assessment of the Human and Economic Hazard from Impact-generated Tsunami." *Natural Hazards*, 38, pp. 355-374. Springer, 2006.

2.4.6-229 Salamon, A., T. Rockwell, S.N. Ward, E. Guidoboni, and A. Comastri, "Tsunami Hazard Evaluation of the Eastern Mediterranean: Historical Analysis and Selected Modeling," *Bulletin of the Seismological Society of America*, Vol. 97, No. 3, pp. 705-724, June 2007.

2.4.6-230 Silver, Eli, S. Day, S.N. Ward, G. Hoffmann, P. Llanes, N. Driscoll, B. Applegate, and S. Saunders, "Volcano Collapse and Tsunami Generation in the Bismarck Volcanic Arc, Papua New Guinea," *Journal of Volcanology and Geothermal Research*, Vol. 186, Issues 3-4, pp. 210-222, October 10, 2009.

2.4.6-231 Gerardi. F., M.S. Barbano, P.M. De Martini, and P. Pantosti, "Discrimination of Tsunami Sources (Earthquake versus Landslide) on the Basis of Historical Data in Eastern Sicily and Southern Calabria," *Bulletin of the Seismological Society of America*, Vol. 98, No. 6, pp. 2795-2805, December 2008.

2.4.6-232 Ward, S.N., "Tsunamis," *Encyclopedia of Physical Science and Technology*, Third Edition, Vol. 17, Academic Press, pp. 175-191, 2002.

2.4.6-233 Ward, S.N., and E. Asphaug, "Asteroid Impact Tsunami of 2880 March 16," *Geophysical Journal international*, 153, pp. F6-F10, February 19, 2003.

2.4.6-234 Ward, S.N., and S. Day, "Tsunami Balls: A Granular Approach to Tsunami Runup and Inundation," *Communications in Computational Physics*, Vol. 3(1), pp. 222-249, January 2008.

2.4.6-235 U.S. Geologic Survey, "Evaluation of Tsunami Sources with the Potential to Impact the U.S. Atlantic and Gulf Coasts," An Updated Report to the Nuclear Regulatory Commission by Atlantic and Gulf of Mexico Tsunami Hazard Assessment Group, 2008.

2.4.6-236 Ward, S.N., "Landslide Tsunami," *Journal of Geophysical Research*, V1.8, November 20, 2000.

2.4.6-237 Ward, S.N., "Tsunami," *Encyclopedia of Solid Earth Geophysics*, Springer Press, 2010.

2.4.6-238 Ward, S.N., and S. Day, "The 1958 Lituya Bay Landslide and Tsunami - A Tsunami Ball Approach," *Journal of Earthquake and Tsunami*, V2.5, November 19, 2009.

2.4.6-239 Ward, S.N. and S. Day, "The 1963 Landslide and Flood at Vaiont Reservoir Italy – A tsunami ball simulation," In preparation, PDF: http://es.ucsc.edu/~ward/papers/Vaiont.pdf, March 5, 2010.

2.4.6-240 Institute of Geological and Nuclear Sciences, *Review of Tsunami Hazard and Risk in New Zealand*, Client Report compiled by Kelvin Berryman, 2006.

2.4.6-241 U.S. Geologic Survey, "A Summary of Findings of the West-Central Florida Coastal Studies Project," Website, http://pubs.usgs.gov/of/2001/of01-303/geology.html, accessed February 23, 2010.

LNP COL 2.4-2

TABLE 2.4.6-201 (SHEET 1 OF 13)
VERIFIED AND PROBABLE CARIBBEAN TSUNAMIS (1498 – 2000)

Origin Data				Effects Data		
Date	**Lat. Long.**	**Earthquake Magnitude**	**Area**	**Location of Effect**	**Runup (m)**	**Deaths**
1530 09 01	10.7N 64.1W	MMI=X	Venezuela	Venezuela:		
[14:30 UT]				Paria	7.3	
				Cumana	6.0	
				Cubagun Island	6.0	
				Gulf of Cariaco		
1690 04 16	17.5N 61.5W	M_S 8.0	Leeward Is.	U.S. Virgin Islands:		
				St. Thomas:		
				Charlotte Amalie		
				Nevis:		
				Charleston		
1692-06-07	17.8N 76.7W	M_S 7.7	Jamaica	Jamaica:		
[11:43 LT]				Port Royal	1.8	2000
				Liganee (Kingston)		
				Saint Ann's Bay		
1751-10-18	18.5N 70.7W	M_S 7.3	Hispaniola	Hispaniola:		
[19:00 UT]				Azua de Compostela		
				Santa Domingo		
				Santa Cruz El Seybo		

LNP COL 2.4-2

TABLE 2.4.6-201 (SHEET 2 OF 13)
VERIFIED AND PROBABLE CARIBBEAN TSUNAMIS (1498 – 2000)

Origin Data				Effects data		
Date	**Lat. Long.**	**Earthquake Magnitude**	**Area**	**Location of Effect**	**Runup (m)**	**Deaths**
1755-11-01	36.0N 11.0 W	MMI = XI	Lisbon, Portugal	Netherlands Antilles		
[9:50 LT]				Saba	7.0	
				St. Martin	4.5	
				Antigua	3.6	
				Dominica	3.6	
				Barbados	1.5-1.8	
				Martinique		
				Cuba:		
				Santiago de Cuba		
1755-11-18	42.7N 70.3W	VIII	Cape Ann, Massachusetts	St. Martins, West Indies		
1761-03-31	37.0N I0.0W	MMI = IX	Lisbon, Portugal	Barbados	1.2	
[12:05 LT]						
1767-04-24	14.4N 61.OW		Martinique and	Martinique		
[6:00 UT]			Barbados	Barbados		
1770-06-03	18.3N 72.2W		Haiti	Golfe de la Gonave and Arcahaie		
[19:15 LT]						
1802-05-05	9.2N 61.5W		Venezuela	Venezuela: Orinoco River		
1823-11-30	14.4N 61.OW		Martinique	Martinique:		
[3: 10 LT]				Saint-Pierre Harbor		

LNP COL 2.4-2

TABLE 2.4.6-201 (SHEET 3 OF 13)
VERIFIED AND PROBABLE CARIBBEAN TSUNAMIS (1498 – 2000)

Origin Data				Effects Data		
Date	**Lat. Long.**	**Earthquake Magnitude**	**Area**	**Location of Effect**	**Runup (m)**	**Deaths**
1842-05-07	19.IN 72.8W	M_S 7.7	Haiti	Haiti:		-5000
[17:30 LT]				Mole St. Nicolas		
				Cap Haitien		
				Port-de-Paix	5.0	200-300
				Forte-Liberte		
				Santiago De 10s Caballeros		
				Dominican Republic		
				Santa Domingo	2.0	
				U.S. Virgin Islands		
				St. John	3.1	
				North coast of Hispaniola	2	
1843-02-08	16.5N 62.2W	MMI=IX	Guadeloupe	Antigua	1.2	
[14:50 UT]						
1853-07-15	12.1N 63.6W	M_S 6.7	Venezuela	Venezuela:		
				Cumana		
				Puerto Sucre		
				Sabana de Caiguire		
				Sabana de Salgado		

LNP COL 2.4-2

TABLE 2.4.6-201 (SHEET 4 OF 13)
VERIFIED AND PROBABLE CARIBBEAN TSUNAMIS (1498 – 2000)

Origin Data				Effects Data		
Date	**Lat. Long.**	**Earthquake Magnitude**	**Area**	**Location of Effect**	**Runup (m)**	**Deaths**
1856-08-09	16.0N 88.0W	M_S 7.5	Honduras	Honduras:	5.0	
				Rio Patuca		
				Omoa		
				Cortez		
				Atlantida		
				Trujillo		
1860-03-08	19.0N 72.0W		Hispaniola	Hispaniola:		
				Golfe de la Gonave		
				Les Cayes		
				Acquin		
				Anse -A-Veau		
1867-11-18	18.0N 65.5W	M_S 7.5	St. Croix and St.	Guadeloupe:	19.8	
[18:45 UT]			Thomas, U.S.	Dechaies	18.3	23
			Virgin Islands	Basse-Terre	1.0	
				Sainte-Rose	10.0	
				Isles des Saintes		
				Grande Terre		
				Fond-du-Cure	1	
				Pointe-a-Pure		

LNP COL 2.4-2

TABLE 2.4.6-201 (SHEET 5 OF 13)
VERIFIED AND PROBABLE CARIBBEAN TSUNAMIS (1498 – 2000)

Origin Data				Effects Data		
Date	Lat. Long.	Earthquake Magnitude	Area	Location of Effect	Runup (m)	Deaths
				U.S. Virgin Islands:		
				St. Thomas:		
				Charlotte Amalie	4.5-6.0	12
				Hassle Island	4.9	
				Altona		
				St. John		
				St. Croix:	7.0-9.0	
				Christiansted		
				Frederiksted	7.6	5
				Gallows Bay		
				Puerto Rico:	1.0-6.0	
				Arroyo	0.9-1.5	
				San Juan	0.9-1.5	
				Vieques Islands	6.1	
				Fajardo		
				Puerto Yabucoa	1.37	
				British Virgin Islands:		
				Peter Island	1.2-1.5	

LNP COL 2.4-2

TABLE 2.4.6-201 (SHEET 6 OF 13)
VERIFIED AND PROBABLE CARIBBEAN TSUNAMIS (1498 – 2000)

Origin Data				Effects Data		
Date	Lat. Long.	Earthquake Magnitude	Area	Location of Effect	Runup (m)	Deaths
				Tortola		
				Road town	1.5	
				Netherrlands Antilles:		
				Saba		
				St. Kitts and Nevis:		
				St. Christoopher (St. Kitts)		
				Netherlands and France		
				St. Martin		
				France		
				St. Barthelemy		
				Antigua and Barbuda:		
				St. Johns	2.4-3.0	
				Martinique	3.0	
				St. Vincent and the Grenadines:		
				Becquina	1.8	
				Grenada:	3.0	
				St. Georges	1.5	
				Charlotte Town (Gouyave)	3.0	
				Venezuela		
				Maiquetia Island		

LNP COL 2.4-2

TABLE 2.4.6-201 (SHEET 7 OF 13)
VERIFIED AND PROBABLE CARIBBEAN TSUNAMIS (1498 – 2000)

Origin Data				Effects Data		
Date	**Lat. Long.**	**Earthquake Magnitude**	**Area**	**Location of Effect**	**Runup (m)**	**Deaths**
1882-09-07	1.3N 77.8W	M_S 8.0	Panama	Panama:		
[7:50 UT]				San Bias Archipelago	3.0	75-100
1883-08-27	5.8s 106.3E		Krakatoa,	U.S. Virgin Islands:		
[10:00 LT]			Indonesia	St. Thomas		
1887-09-23	19.7N 74.4W		Haiti	Haiti:		
[12:00 UT]				Mole-Saint-Nicolas		
				Jeremie		
				Anse-d'Hainault		
				Point Tiburon		
1900-10-29	10.9N 66.8W	M_S 8.4	Venezuela	Venezuela		
				Macuto		
				Puerto Tuy	10.0	
1902-08-30	14.4N 61.0W		Martinique	Martinique	1.0	
[21:25 LT]				Fort-de-France		
1906-01-31	2.4N 19.3W	M_S 8.9	Venezuela	Venezuela:		
[15:36 UT]				Cumana		
				Campano		
				Costas Nueva Esparta		
				Rio Caribe		
				Isla de Margarita		

TABLE 2.4.6-201 (SHEET 8 OF 13)
VERIFIED AND PROBABLE CARIBBEAN TSUNAMIS (1498 – 2000)

Origin Data				Effects Data		
Date	**Lat. Long.**	**Earthquake Magnitude**	**Area**	**Location of Effect**	**Runup (m)**	**Deaths**
1907-01-14	8.1N 76.7W	M_S 6.5	Jamaica	Jamaica:		
[21:36 UT]				Hope Bay	2.5	
				Orange Bay	2.5	
				Sheerness Bay	2.5	
				St. Ann's Bay	2.5	
				Annotto Bay	1.8-2.4	
				Port Maria	1.8-2.4	
				Ocho Rios		
				Bluff Bay		
				Port Antonia		
				Kingston	2.5	
1911-11-03	10.5N 61.2W		Trinidad	Trinidad		
1916-04-24	11.0N 85.0W	M_S 7.6	Panama	Panama:		
[8:02 UT]				Almirante		
				Bocas del Toro		
				Isla de Carenero		
				Isla Bastimento		

TABLE 2.4.6-201 (SHEET 9 OF 13)
VERIFIED AND PROBABLE CARIBBEAN TSUNAMIS (1498 – 2000)

Origin Data				Effects Data		
Date	**Lat. Long.**	**Earthquake Magnitude**	**Area**	**Location of Effect**	**Runup (m)**	**Deaths**
1918-10-11	18.5N 61.5W	M_S 7.5	Puerto Rico	Puerto Rico:		140
[4:14 UT]				Aguadilla	2.4-3.4	32
				Punta Agujereada	5.5-6.1	8
				Punta Higuero	5.2	
				800 m SE of Punta Higuero	2.6-2.7	
				Punta Borinquen	4.5	
				Isla Mona	3.0	
				Rio Culebrinas	4.0	
				Bahia de Boqueron	0.9	
				800 m SE at bay entrance	0.4	
				Isabella	2.0	
				Cayo Cardona	0.75	
				Guanica	0.5	
				Mayaguez	1.5	
				Isla Caja de Muertos	1.5	
				Puerto Arecibo	0.6	
				Rio Grande	0.1	
				Rio Grande de Loiza	1.0	
				Playa Ponce		

TABLE 2.4.6-201 (SHEET 10 OF 13)
VERIFIED AND PROBABLE CARIBBEAN TSUNAMIS (1498 – 2000)

Origin Data				Effects Data		
Date	**Lat. Long.**	**Earthquake Magnitude**	**Area**	**Location of Effect**	**Runup (m)**	**Deaths**
				St. Thomas		
				Krum Bay	1.2	
				Charlotte Amalie	0.45	
				Dominican Republic		
				Santo Domingo (Rio Ozama)	0.7	
				U.S. Virgin Islands	0.3-0.6	
				Tortola		
1918-10-24	18.5N 67.5W		Puerto Rico	Mona Passage		
[3:43 UT]				Puerto Rico		
				Texas		
				Galveston		
1929-01-17	10.6N 65.6W	M_S 6.9	Venezuela	Venezuela:		
[11:52 UT]				Cumana		
				Manicuare		
				El Dique		
				El Barbudo		
				El Salado		
				Puerto Sucre		

TABLE 2.4.6-201 (SHEET 11 OF 13)
VERIFIED AND PROBABLE CARIBBEAN TSUNAMIS (1498 – 2000)

Origin Data				Effects Data		
Date	**Lat. Long.**	**Earthquake Magnitude**	**Area**	**Location of Effect**	**Runup (m)**	**Deaths**
1939-08-15	22.5N 79.2W	M_S 8.1	Cuba	Cuba:		
[3:52 UT]				Cayo Frances		
1946-08-04	19.3N 68.9W	M_S 8.1	Dominican	Dominican Republic:		
[17:51 UT]			Republic, Haiti	Matancitas	2.5	1790
			and Puerto Rico	Julia Molina	4.0-5.0	
				Cabo Samana		
				Puerto Rico:		
				San Juan		
				Bermuda		
				Florida:		
				Daytona Beach		
				New Jersey:		
				Atlantic City		
1946-08-08	19.5N 69.5W	M_S 7.9	Puerto Rico	Puerto Rico:		75
[3:28 UT]				Aguadilla		
				Mayaguez		
				San Juan		
				Bermuda		
				Florida:		

TABLE 2.4.6-201 (SHEET 12 OF 13)
VERIFIED AND PROBABLE CARIBBEAN TSUNAMIS (1498 – 2000)

Origin Data				Effects Data		
Date	Lat. Long.	Earthquake Magnitude	Area	Location of Effect	Runup (m)	Deaths
				Daytona Beach		
				New Jersey		
				Atlantic City		
1969-12-25	15.8N 59.1W	M_S 7.6	Leeward Is.	Barbados	0.46	
[21:32 UT]				Antigua	0.3	
				Dominica	0.12	
1985-03-16	17.0N 62.4W	M_S 6.8	Leeward Is.	Guadeloupe	0.1	
14:54				Basse-Terre		
1989-11-01	19.0N 68.8W	M_b 5.2	Costa Rica	Panama:		
[10:25 UT]				Bocas del Toro	0.6	
				Isla de Carenero		
				San Cristobal Island		
				Bastimento	0.1	
				Cristobal	0.1	
				Portobelo	0.6	
				Colon		
				Coca Solo	0.8	
				Costa Rica		
				Limon		

TABLE 2.4.6-201 (SHEET 13 OF 13)
VERIFIED AND PROBABLE CARIBBEAN TSUNAMIS (1498 – 2000)

Origin Data				Effects Data		
Date	**Lat. Long.**	**Earthquake Magnitude**	**Area**	**Location of Effect**	**Runup (m)**	**Deaths**
				Punta Cahuita-Puerto Viejo	2.0	
				U.S. Virgin Islands		
				St. Croix		
				Limetree	0.07	
1997-07-09	10.6N 63.5W	M_w 7.0	Venezuela	Venezuela:		
[19:24 UT]				Isla de Margarita		
				Tobago		
1997-12-26	16.7N 62.2W		Montserrat	Montserrat	3.0	
[3:00 LT]						

Notes:
LT = local time
m = meter
MMI = Modified Mercalli Intensity
M_S = surface-wave magnitude
M_w = moment magnitude
UT = universal time

Source: Reference 2.4.6-209

LNP COL 2.4-2

Table 2.4.6-202 (Sheet 1 of 3)
Tsunami Events Affecting the Caribbean

Date						Tsunami Cause				Tsunami Source Location				Tsunami Parameters						Tsunami Effects				
																Magnitude								
Year	Month	Day	Hour	Minute	Sec.	Validity[a]	Source Code[b]	Earthquake Magnitude	Volcano	Country	Name	Latitude	Longitude	Max Water Height	Num. of Runups	Abe	Iida	Tsunami Intervals	Warn Status	Number of Deaths	Number of Injuries	Damage (Millons of Dollars)	Number of Houses Destroyed	Photos
1530	9	1	14	30		4	1	*		Venezuela	Cumana	11	-64	7.3	3		2.6							
1690	4	16				4	1	8		Antigua And Barbuda	Antigua; Saint Kitts And Nevis	18	-62		3									
1692	6	7				4	3	7.7		Jamaica	Port Royal	18	-77	1.8	4					2000				
1755	11	1				4	1	*		Portugal	Lisbon	36	-11	30	52		3.6							
1761	3	31	12	5		4	1	*		Portugal	Lisbon	37	-10	2.4	11		1.3							
1767	4	24	6			3	1	*		Martinique	Martinique & Barbados	14	-61		2									
1770	6	3				4	1	*		Haiti	Port-Au-Prince	19	-72		4									
1775	2	11				3	1	*		Cuba	Santiago De Cuba	20	-76		2									
1802	8	15				3	1	*		Venezuela	Cumana	10	-64		1									
1823	11	30				4	1	*		Martinique	Saint Pierre	14	-61		1									
1842	5	7				4	1	7.7		Haiti	Cap-Haitian	20	-72	5	8		4.2			300				
1843	2	8	14	50		4	1	8.3	Volcano	Guadeloupe	Pointe-A-Pitre	17	-62	1.2	1		0.3							
1853	7	15				3	1	6.7		Venezuela	Cumana	11	-64		4					113				
1856	8	9				4	1	7.5		Honduras	Omoa	16	-88	5	5									
1860	4	8				4	1	7.5		Haiti	Anse-A-Veau	19	-73		4									
1867	11	18	18	45		4	1	7.5		USA Territory	Virgin Islands	18	-65	10	33		2.3			30				
1868	3	17	11	37		3	1	*		USA Territory	Virgin Islands	18	-65	1.5	5		-1							
1882	9	7	7	50		4	3	7.9		Panama	San Blas Archipelago	9.5	-79	3	4			1		100				
1883	8	27	2	59		4	6		Volcano	Indonesia	Krakatau	-6	105	35	75		5.1	5		36,500				
1887	9	23	12			4	1	*		Haiti	Mole Saint-Nicolas	20	-74		4									
1900	10	29				3	1	8.4		Venezuela	Mancuto	11	-67	10	4									
1902	5	5				4	7		Volcano	Martinique	Mont Pelee	15	-61	5	1									
1902	5	7				4	6		Volcano	Saint Vincent And The Grenadines	Soufriere Volcano	13	-61		3									
1902	8	30				4	6		Volcano	Martinique	Mount Pelee	15	-61	1	1									

LNP COL 2.4-2

Table 2.4.6-202 (Sheet 2 of 3)
Tsunami Events Affecting the Caribbean

Date						Tsunami Cause				Tsunami Source Location				Tsunami Parameters					Tsunami Effects					
																Magnitude								
Year	Month	Day	Hour	Minute	Sec.	Validity[a]	Source Code[b]	Earthquake Magnitude	Volcano	Country	Name	Latitude	Longitude	Max Water Height	Num. of Runups	Abe	Iida	Tsunami Intervals	Warn Status	Number of Deaths	Number of Injuries	Damage (Millons of Dollars)	Number of Houses Destroyed	Photos
1906	1	31				4	1	*		Venezuela	Caracas	11	-67		6									
1907	1	14	21	36		4	1	6.5		Jamaica	Jamaica	18	-77	2.5	10		1.3							
1911	11	3				3	6		Volcano	Trinidad And Tobago	Trinidad	11	-61		1									
1916	4	25	8	2		4	1	7.6		Panama	Bocas Del Toro	9.3	-82	1.3	5									
1918	10	11	14	14	30	4	1	7.3		USA Territory	Puerto Rico: Mona Passage	19	-68	6.1	21		2.6			142		4		
1918	10	24	3	43		4	1	*		USA Territory	Puerto Rico	19	-68		2									
1929	1	17	11	52		4	1	6.9		Venezuela	Cumana	11	-66		5									
1929	11	18	20	32		4	3	7.4		Canada	Grand Banks, Newfoundland	45	-56	7	45		2.2			28		1		
1946	8	4	17	51	6	4	1	8.1		Dominican Republic	Northeastern Coast	19	-69	5	8		2.2			1790				
1946	8	8	13	28		4	1	7.9		Dominican Republic	Northeastern Coast	20	-70	0.6	13					75				
1967	7	29	23	59	59	4	1	6.5		Venezuela	Caracas	11	-67	0.1	1									
1969	12	25	21	32		4	1	7.6		Guadeloupe	Grand Bourg	16	-60	0.5	3		-3							
1985	3	16	14	54	0.7	4	1	6.4		Guadeloupe	Guadeloupe	17	-62	0.1	1		-3							
1989	11	1	10	25	52	3	1	4.4		USA Territory	Puerto Rico	19	-69	0.1	1									
1991	4	22	21	56	52	4	1	7.7		Costa Rica	Limon, Pandora	9.7	-83	3	21		1			2				
1997	7	9	19	24	13	3	1	7		Venezuela	Cariaco-Cumana	11	-63		1									
1997	12	26	8			4	7		Volcano	Montserrat	White River Valley	17	-62	3	1									
1999	1	20				4	6		Volcano	Montserrat	Soufriere Hills Volcano	17	-62	2	3									

LNP COL 2.4-2

Table 2.4.6-202 (Sheet 3 of 3)
Tsunami Events Affecting the Caribbean

Date						Tsunami Cause				Tsunami Source Location				Tsunami Parameters						Tsunami Effects				
																Magnitude								
Year	Month	Day	Hour	Minute	Sec.	Validity[a]	Source Code[b]	Earthquake Magnitude	Volcano	Country	Name	Latitude	Longitude	Max Water Height	Num. of Runups	Abe	Iida	Tsunami Intervals	Warn Status	Number of Deaths	Number of Injuries	Damage (Millons of Dollars)	Number of Houses Destroyed	Photos
2003	7	12				4	6		Volcano	Montserrat	Soufriere Hills Volcano	17	-62	4	5									
2004	11	21	11	41	7.7	4	1	6.3		Guadeloupe	Basse-Terre, Les Saintes	16	-62	0.7	7									
2004	12	26	0	58	53	4	1	9		Indonesia	Off W. Coast Of Sumatra	3.3	96	50	716				4	250,000		10,000		39
2006	5	20	11	20		4	6		Volcano	Montserrat	Soufriere Hills Volcano	17	-62	1	4				4					

Notes:

Abe = Abe defined two different tsunami magnitude amplitudes. His first tsunami magnitude (1979) is Mt = logH + B, where H is the maximum single crest or trough amplitude of the tsunami waves (in meters) and B a constant. The second definition (1981) is Mt = logH + alogR + D, where R is the distance in km from the earthquake epicenter to the tide station along the shortest oceanic path, and a and D are constants.
Iida = Iida and others (1967) defined tsunami magnitude (M) as M = log2h, where "h" is the maximum runup height of the wave.

(a)Validity:
0 = erroneous entry
1 = very doubtful tsunami
2 = questionable tsunami
3 = probable tsunami
4 = definite tsunami

(b)Source Code:
0 = Unknown Cause
1 = Earthquake
2 = Questionable Earthquake
3 = Earthquake and Landslide
4 = Volcano and Earthquake
5 = Volcano, Earthquake, and Landslide
6 = Volcano
7 = Volcano and Landslide
8 = Landslide
9 = Meteorological
10 = Explosion
11 = Astronomical Tide

Source: Reference 2.4.6-206

LNP COL 2.4-2

Table 2.4.6-203
Tsunami Events Affecting the Gulf of Mexico

Date						Tsunami Cause				Tsunami Source Location				Tsunami Parameters						Tsunami Effects				
																Magnitude								
Year	Month	Day	Hour	Minute	Sec.	Validity [a]	Source Code[b]	Earthquake Magnitude	Volcano	Country	Name	Latitude	Longitude	Max Water Height	Num. of Runups	Abe	Iida	Tsunami Intervals	Warn Status	Number of Deaths	Number of Injuries	Damage (Millons of Dollars)	Number of Houses Destroyed	Photos
1918	10	24	3	43		4	1			USA Territory	Puerto Rico	18.5	-68		2									
1964	3	28	3	36	14	4	3	9.2		USA	Prince William Sound, AK	61.1	-148	67	373		6.1	5		221		124		8

Notes:

[a]Validity:
0 = erroneous entry
1 = very doubtful tsunami
2 = questionable tsunami
3 = probable tsunami
4 = definite tsunami

[b]Source Code:
0 = Unknown Cause
1 = Earthquake
2 = Questionable Earthquake
3 = Earthquake and Landslide
4 = Volcano and Earthquake
5 = Volcano, Earthquake, and Landslide
6 = Volcano
7 = Volcano and Landslide
8 = Landslide
9 = Meteorological
10 = Explosion
11 = Astronomical Tide

Source: Reference 2.4.6-206

LNP COL 2.4-2

Table 2.4.6-204 (Sheet 1 of 2)
Mareogram Summary for Tsunami Source 1: Puerto Rico Trench

Location	Region	Travel Time (hr-min)	Peak Height (cm)	Initial Motion	Period (hr-min)
Brownsville, TX	Gulf	6 hr. 22 min	4	depression	2 hr. 3 min
Corpus Christi, TX	Gulf	6 hr. 45 min	4	depression	1 hr. 18 min
Galveston, TX	Gulf	8 hr. 2 min	6	depression	1 hr. 58 min
High Island, TX	Gulf	8 hr. 30 min	3	depression	1 hr. 57 min
Eugene Island, LA	Gulf	8 hr. 10 min	3	depression	1 hr. 56 min
Port Fourchon, LA	Gulf	5 hr. 52 min	10	depression	2 hr. 3 min
Grand Isle, LA	Gulf	6 hr.	12	depression	1 hr. 38 min
Waveland, MS	Gulf	10 hr. 36 min	1	depression	
Biloxi, MS	Gulf	8 hr. 28 min	5	depression	2 hr. 5 min
MS – AL Border	Gulf	9 hr. 35 min	3	depression	2 hr. 2 min
Destin, FL	Gulf	5 hr. 38 min	7	depression	1 hr. 55 min
Suwanee, FL	Gulf	8 hr. 37 min	3	depression	2 hr. 2 min
Panama Beach, FL	Gulf	5 hr. 47 min	5	depression	1 hr. 54 min
Panama City, FL	Gulf	6 hr. 20 min	11	depression	2 hr. 2 min
Clearwater Beach, FL	Gulf	6 hr. 58 min	8	depression	1 hr. 6 min
St Petersburg, FL	Gulf	7 hr. 48 min	5	depression	2 hr. 56 min
Tampa, FL	Gulf	8 hr. 28 min	5	depression	2 hr. 28 min
Port Manatee, FL	Gulf	7 hr. 28 min	5	depression	1 hr. 28 min
Bonita, FL	Gulf	7 hr. 37 min	25	depression	1 hr. 50 min
Naples, FL	Gulf	7 hr. 28 min	23	depression	1 hr.
Virginia Key, FL	Atlantic	2 hr. 57 min	15	elevation	49 min
Ocean Reef, FL	Atlantic	3 hr. 13 min	28	elevation	1 hr. 40 min
Jupiter, FL	Atlantic	2 hr. 47 min	54	elevation	1 hr. 2 min
Flagler, FL	Atlantic	4 hr. 18 min	117	elevation	1 hr. 10 min
Vaca Key, FL	Atlantic	4 hr.	13	elevation	1 hr. 11 min
St Simons, GA	Atlantic	5 hr. 30 min	40	elevation	1 hr. 13 min
Altamaha, GA	Atlantic	5 hr. 33 min	47	elevation	1 hr. 15 min
So Santee, SC	Atlantic	4 hr. 32 min	77	elevation	1 hr. 22 min

LNP COL 2.4-2

Table 2.4.6-204 (Sheet 2 of 2)
Mareogram Summary for Tsunami Source 1: Puerto Rico Trench

Location	Region	Travel Time (hr-min)	Peak Height (cm)	Initial Motion	Period (hr-min)
Springmaid, SC	Atlantic	4 hr. 57 min	129	elevation	1 hr. 8 min
Charleston, SC	Atlantic	4 hr. 57 min	49	elevation	1 hr. 15 min
Surf City, NC	Atlantic	4 hr. 23 min	112	elevation	1 hr. 8 min
Beaufort, NC	Atlantic	3 hr. 38 min	147	elevation	45 min
Oregon Inlet, NC	Atlantic	3 hr. 45 min	38	elevation	42 min
Duck, NC	Atlantic	3 hr. 57 min	140	elevation	drained
Currituck, NC	Atlantic	4 hr. 15 min	102	elevation	36 min
Chesapeake B, VA	Atlantic	7 hr. 12 min	6	elevation	46 min
Annapolis, MD	Atlantic	10 hr. 28 min	3	elevation	~2 hr.
Cape Henlopen, DE	Atlantic	4 hr. 52 min	64	elevation	42 min
Cape May, NJ	Atlantic	5 hr.	68	elevation	45 min
Atlantic City, NJ	Atlantic	4 hr. 45 min	155	elevation	45 min
Montauk, NY	Atlantic	4 hr. 48 min	68	elevation	16 min
Bar Harbor, ME	Atlantic	5 hr. 33 min	71	elevation	6 min
D41424 (32.4N, 73W)	Atlantic	1 hr. 52 min	35	elevation	
D41420 (23.3N, 67.6W)	Atlantic	32 min	131	elevation	
D41421 (23.4N, 63.9W)	Atlantic	31 min	175	elevation	
D7-2 (38.6N, 68 W)	Atlantic	2 hr. 10 min	78	elevation	
D42407 (23.4N, 63.9W)	Caribbean	10 min	-61	depression	
D8-1 (25.4N, 86.8W)	Gulf	3 hr. 27 min	-2	depression	
Bermuda	Atlantic	1 hr. 57 min	511	elevation	12 min
Limetree, St Croix	Caribbean	1 min	240	depression	15 min
Punta, Guayanilla	Caribbean	0 min	173	elevation	21 min

Notes:
hr. = hour
min = minute
cm = centimeter
Source: Reference 2.4.6-225

LNP COL 2.4-2

Table 2.4.6-205
Source Parameters and Range of Average Slip and Moment Magnitudes of Earthquakes from which Tsunami Simulations Were Computed by USGS

Fault #*	Name	Type	Length (km)	Width (km)	Strike (°)	Dip (°)	Rake (°)	Avg. Slip-low (m)	Avg. Slip-high (m)	Moment Magnitude (low)	Moment Magnitude (high)
1	W. Cayman	Oceanic Transform Fault	746	15	N73E	83N	185	10.6	12.4	8.3	8.35
2	E. Cayman	Oceanic Transform Fault	915	15	N77E	80S	175	12.1	14.2	8.4	8.45
3a	Hispaniola	Subduction Zone	525	50	N98E	20S	70	8.2	9.4	8.8	8.84
3b	Puerto Rico	Subduction Zone	385	50	N83E	20S	23				
3c	Virgin Islands	Subduction Zone	485	50	N102E	20S	42				
4a	W. Northern Panama	Oceanic Convergent Boundary	200	40	N113E	30S	90	3.7	4.3	8.24	8.28
4b	E. Northern Panama	Oceanic Convergent Boundary	350	40	N75E	35S	90				
5a	W. Southern Caribbean	Subduction Zone	550	50	N53E	17S	90	4.7	5.4	8.46	8.5
5b	E. Southern Caribbean	Subduction Zone	200	50	N95E	17S	90				

Notes:

* = Faults with same numeral are treated as one tsunami source.
km = kilometer
m = meter

Source: Reference 2.4.6-214

LNP COL 2.4-2

Table 2.4.6-206
Parameters for Worst Case Landslide Tsunamis

Landslide	Area A	Volume V	Thickness of the Unit T	Slide Speed Vs	Initial Wave Amplitude A_0	Water Depth of the Slide Event H_0	Diameter D	Distance of the Measurement Point from the Source R
	(km^2)	(km^3)	(m)	(m/s)	(m)	(m)	(m)	(km)
East Breaks	520	22	42	25	7	1750	25,719	1000
	520	22	42	50	26	1750	25,719	1000
Mississippi Canyon	3720	428	115	25	21	1689	68,822	640
	3720	428	115	50	73	1689	68,822	640
Florida Escarpment	648	16.2	25	25	4	2000	28,724	275
	648	16.2	25	50	14	2000	28,724	275
Slope above the Florida Escarpment	648	16.2	25	7	1.2	600	28,724	325
	648	16.2	25	14	4.1	600	28,724	325

Notes:

km = kilometer
km^2 = square kilometer
km^3 = cubic kilometer
m = meter
m/s = meters per second
Vs = slide velocity

LNP COL 2.4-2

Table 2.4.6-207
Formula-Based Results to Some Worst Case Landslide Tsunamis

Landslide	Exponent φ	Offshore Wave Height at a Distance R from the Source A(R) (m)	Estimated Runup η_{est} (m)	Estimated Run-in Distance X_{est} (mi.)
East Breaks	0.94	0.12	0.8	0.02
	0.94	0.42	2.2	0.08
Mississippi Canyon	0.78	2.06	7.9	0.38
	0.78	7.17	21.4	1.22
Florida Escarpment	0.95	0.23	1.4	0.05
	0.95	0.8	3.8	0.16
Slope above the Florida Escarpment	0.75	0.11	0.6	0.02
	0.75	0.38	1.7	0.06

Notes:

m = meter
mi. = mile

LNP COL 2.4-2

Table 2.4.6-208
Parameters for Worst Case Earthquake Tsunamis

Earthquake Location	Rigidity μ (Pa)	Fault Length L (km)	Fault Width W (km)	Fault Area A (km^2)	Average Fault Slip Δu (m)	Dip Angle ϕ (degree)	Rake Angle ρ (degree)
Mid Gulf	3.0E+10	50	23	1150	1	45	90
Vera Cruz	3.0E+10	199	93	18,507	4	45	90
Venezuela	3.0E+10	550	100	55,000	21.5	17	90

Notes:

degree = degree angle
km = kilometer
km^2 = square kilometer
m = meter
Pa = Pascal

LNP COL 2.4-2

Table 2.4.6-209
Formula-Based Results to Some Worst Case Earthquake Tsunamis

Earthquake Location	Magnitude Mw (Nm)	Water Depth at the Source H0 (m)	Diameter or Physical Size of Uplift D (m)	Distance of the Measurement Point from the Source R (km)	Exponent φ	Offshore Wave Height at a Distance R from the Source A(R) (m)	Estimated Runup η_{est} (m)	Estimated Run-in Distance X_{est} (mi.)
Mid Gulf	7.0	3121	36,500	450	0.96	0.02	0.25	0.01
Vera Cruz	8.2	2836	146,000	1500	0.73	0.22	1.48	0.05
Venezuela	9.0	1847	325,000	2400	0.53	1.33	5.67	0.25

Notes:

km = kilometer
m = meter
mi. = mile
Nm = Newton meter

LNP COL 2.4-2

Table 2.4.6-210
Coincident Runup and Run-in for the Worst Case Landslide Tsunamis

	Without Considering Tides, Wind Waves, and Sea Level Anomalies Corrections		Considering Tides, Wind Waves, and Sea Level Anomalies Corrections	
Name	**Runup η_{est} m (ft.) NAVD88**	**Run-in Distance X_{est} (mi.)**	**Runup η_{est} m (ft.) NAVD88**	**Run-in Distance X_{est} (mi.)**
East Breaks (Vs = 25 m/s)	0.8 (2.6)	0.02	1.9 (6.2)	0.07
East Breaks (Vs = 50 m/s)	2.2 (7.2)	0.08	3.4 (11.2)	0.13
Mississippi Canyon (Vs = 25 m/s)	7.9 (25.9)	0.38	9.0 (29.5)	0.44
Mississippi Canyon (Vs = 50 m/s)	21.4 (70.2)	1.22	22.5 (73.8)	1.29
Florida Escarpment (Vs = 25 m/s)	1.4 (4.9)	0.05	2.5 (8.2)	0.10
Florida Escarpment (Vs = 50 m/s)	3.8 (12.5)	0.16	4.9 (16.0)	0.21
Slope above the Florida Escarpment (Vs = 7 m/s)	0.6 (2.0)	0.02	1.7 (5.6)	0.06
Slope above the Florida Escarpment (Vs = 14 m/s)	1.7(5.6)	0.06	2.8 (9.2)	0.11
Maximum	**21.4 (70.2)**	**1.22**	**22.5 (73.8)**	**1.29**

LNP COL 2.4-2

Table 2.4.6-211
Coincident Runup and Run-in for the Worst Case Earthquake Tsunamis

	Without Considering Tides, Wind Waves, and Sea Level Anomalies Corrections		Considering Tides, Wind Waves, and Sea Level Anomalies Corrections	
Name	**Runup η_{est} m (ft.) NAVD88**	**Run-in Distance X_{est} (mi.)**	**Runup η_{est} m (ft.) NAVD88**	**Run-in Distance X_{est} (mi.)**
Mid Gulf	0.3 (1.0)	0.01	1.4 (4.6)	0.04
Vera Cruz	1.5 (4.9)	0.05	2.6 (8.5)	0.10
Venezuela	5.7 (18.7)	0.25	6.8 (22.3)	0.31
Maximum	**5.7 (18.7)**	**0.25**	**6.8 (22.3)**	**0.31**

Notes:

ft. = feet
mi. = mile
m = meter
Vs = slide velocity

Attachments/Enclosures:

Attachment 02.04.06-A	Figure 2.4.6-228: Morphology of the West Florida Escarpment and the West Florida Slope
Attachment 02.04.06-B	Figure 2.4.6-229: Bathymetric Map of West Florida Shelf and Slope

List of Attachments:

1. Attachment 02.04.05-A: Figure 2.4.5-228: Comparison of Maximum Storm Surge Heights Using HSU Method and SLOSH Model [1 page]
2. Attachment 02.04.05-B: Figure 2.4.5-229: Relationship Between the Coastal Storm Surge Heights and Water Elevations [1 page]
3. Attachment 02.04.05-C: Figure 2.4.5-230: Water Elevation at LNP Site Due to PMH-Induced Surge as Indicated by 1000 Monte Carlo Simulation Runs [1 page]
4. Attachment 02.04.05-D: Figure 2.4.5-231: Wave Setup and Runup Due to Wind-Driven Wave Action as Indicated by 1000 Monte Carlo Simulation Runs [1 page]
5. Attachment 02.04.05-E: Figure 2.4.5-232: Total Water Elevation at LNP Site Due to PMH-Induced Surge and Wave Action as Indicated by 1000 Monte Carlo Simulation Runs [1 page]
6. Attachment 02.04.05-F: Figure 2.4.5-233: Histogram of Total Water Elevation at LNP Site Due to Wave Setup, Runup, and PMH-Induced Surge as Indicated by 1000 Monte Carlo Simulation Runs [1 page]
7. Attachment 02.04.06-A: Figure 2.4.6-228: Morphology of the West Florida Escarpment and the West Florida Slope [1 page]
8. Attachment 02.04.06-B: Figure 2.4.6-229: Bathymetric Map of West Florida Shelf and Slope [1 page]

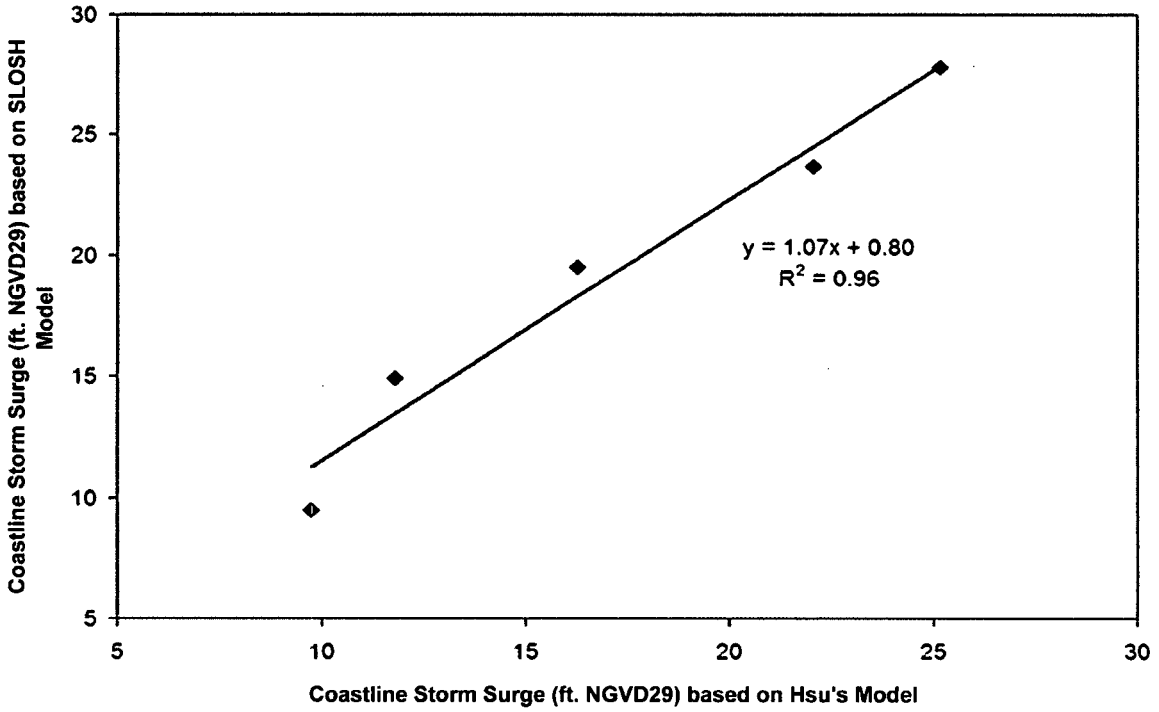

Progress Energy Florida
Levy Nuclear Plant
Units 1 and 2
Part 2, Final Safety Analysis Report

Comparison of Maximum StormSurge Heights Using HSU Method and SLOSH Model
FIGURE 2.4.5-228 Rev 2

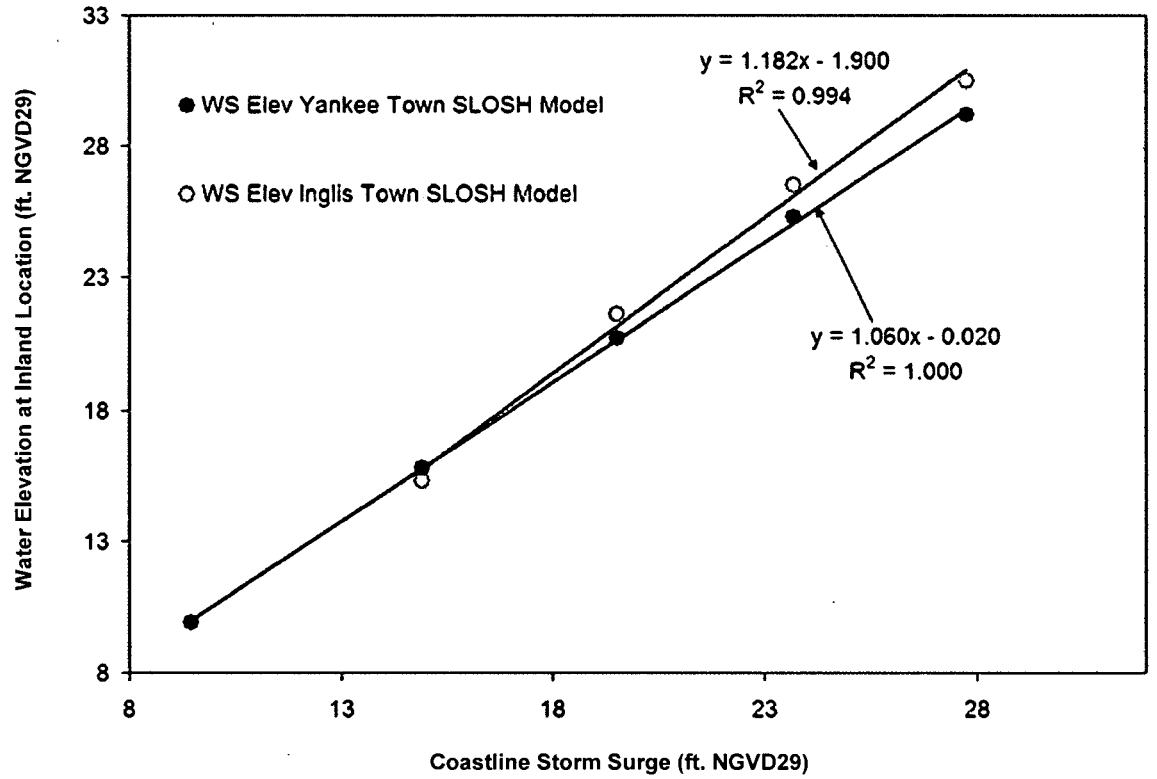

Progress Energy Florida
Levy Nuclear Plant
Units 1 and 2
Part 2, Final Safety Analysis Report

Relationship Between the Coastal Storm Surge Heights and Water Elevations

FIGURE 2.4.5-229 Rev 2

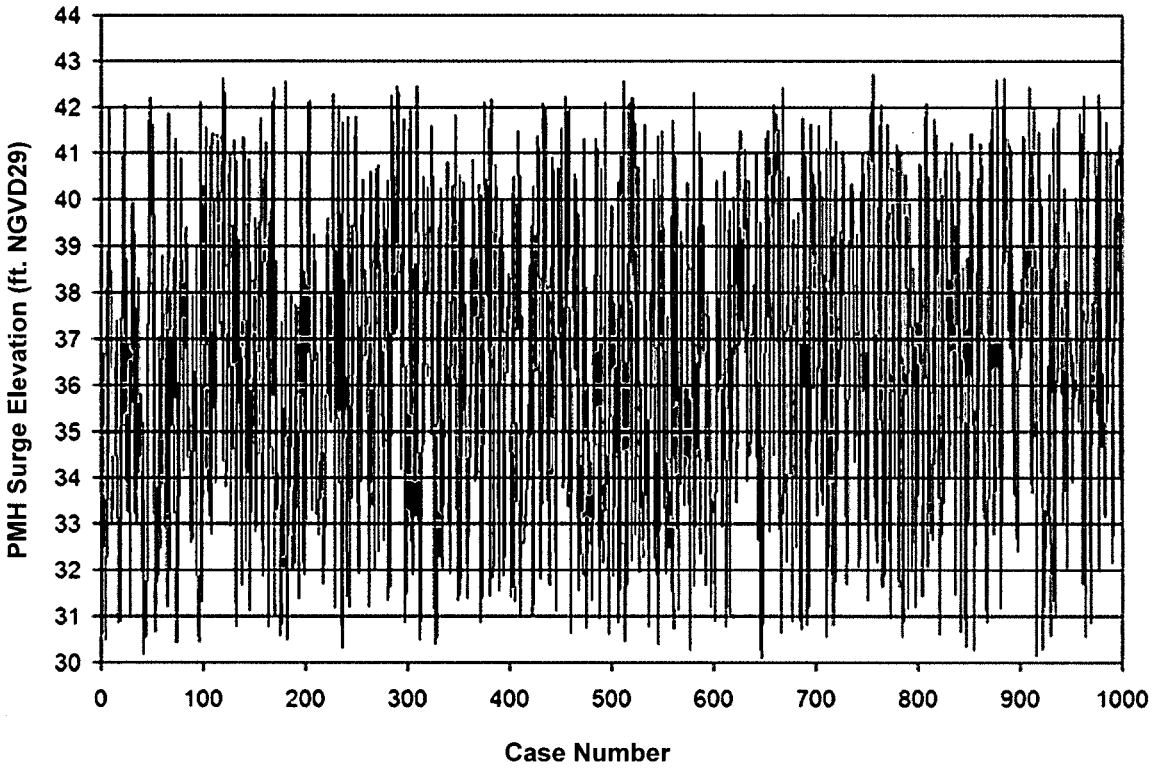

Progress Energy Florida
Levy Nuclear Plant
Units 1 and 2
Part 2, Final Safety Analysis Report

Water Elevation at LNP Site Due to PMH-Induced Surge as Indicated by 1000 Monte Carlo Simulation Runs

FIGURE 2.4.5-230 Rev 2

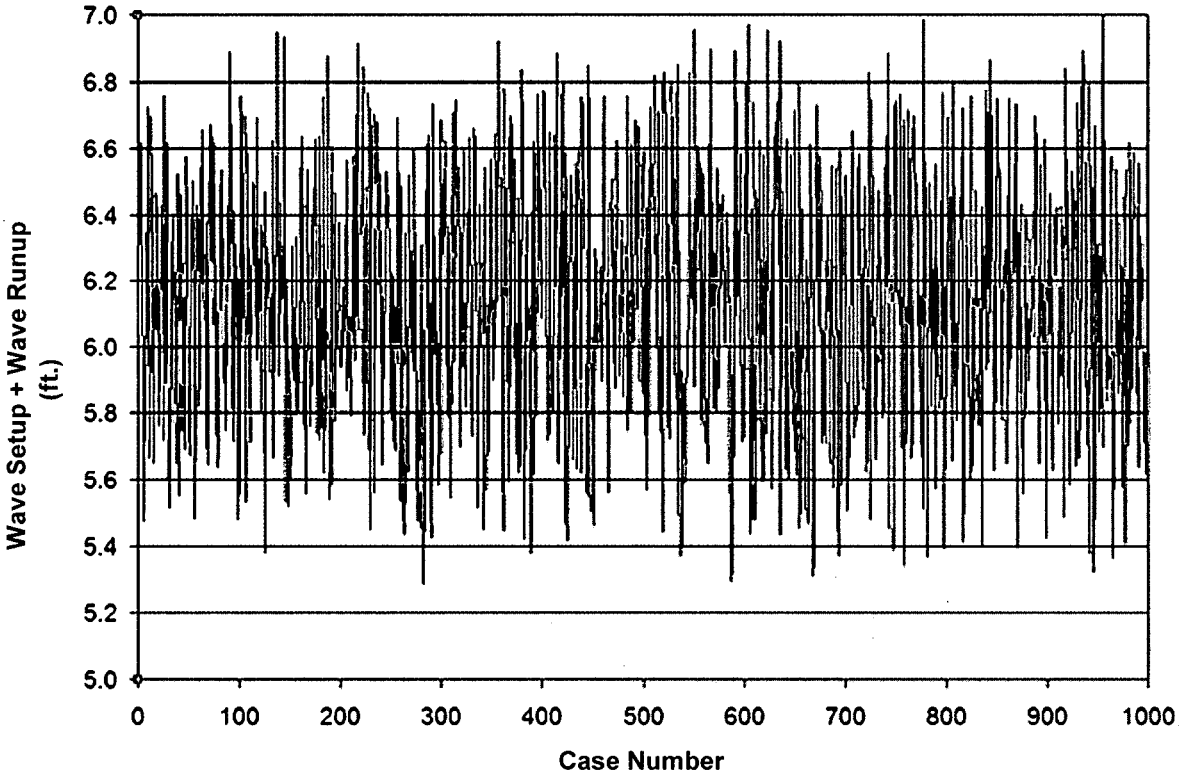

Progress Energy Florida

Levy Nuclear Plant
Units 1 and 2
Part 2, Final Safety Analysis Report

Wave Setup and Runup Due to Wind-Driven Wave Action as Indicated by 1000 Monte Carlo Simulation Runs

FIGURE 2.4.5-231

Rev 2

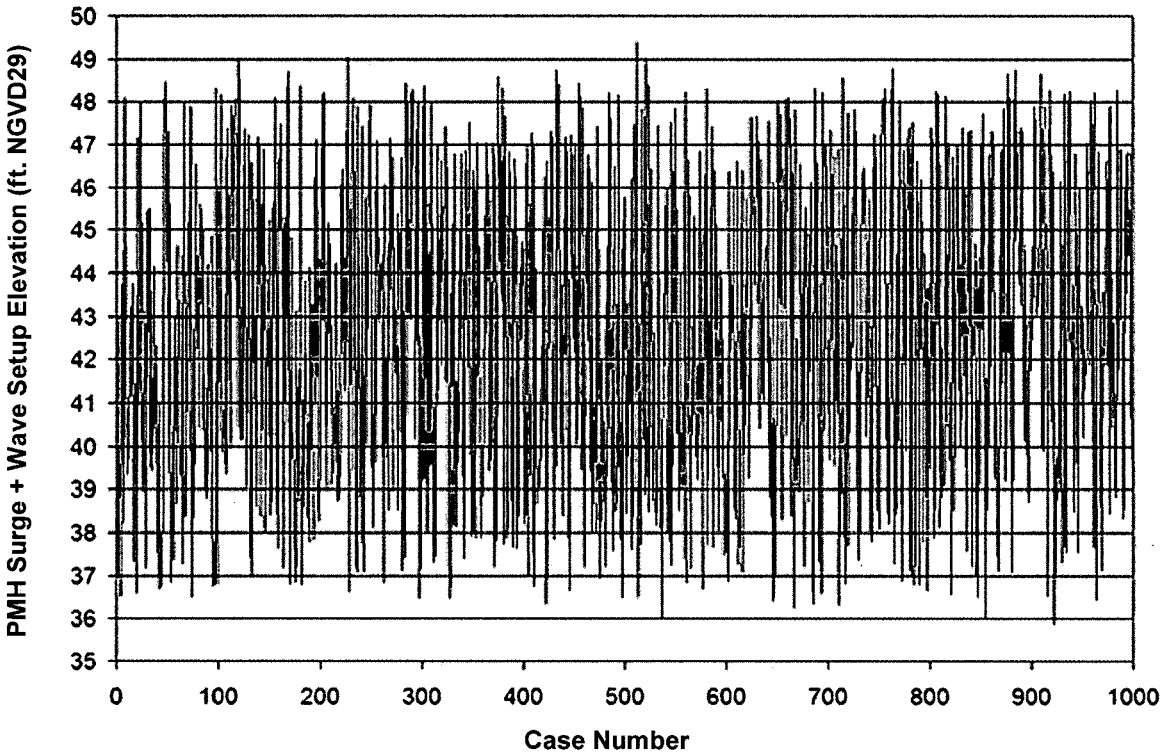

Progress Energy Florida
Levy Nuclear Plant
Units 1 and 2
Part 2, Final Safety Analysis Report

Total Water Elevation at LNP Site Due to PMH-Induced Surge and Wave Action as Indicated by 1000 Monte Carlo Simulation Runs

FIGURE 2.4.5-232 Rev 2

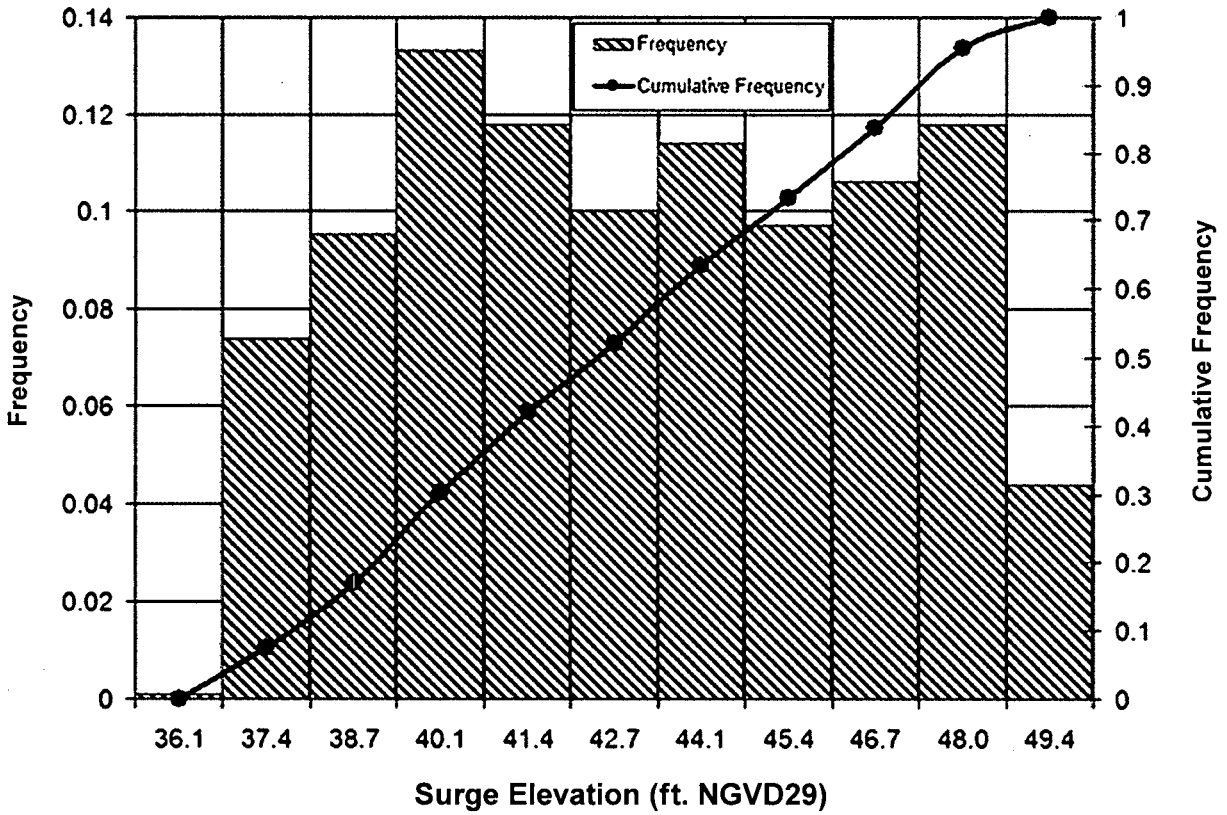

Progress Energy Florida
Levy Nuclear Plant
Units 1 and 2
Part 2, Final Safety Analysis Report

Histogram of Total Water Elevation at LNP Site Due to Wave Setup, Runup, and PMH-Induced Surge as indicated by 1000 Monte Carlo Simulation Runs

FIGURE 2.4.5-233 Rev 2

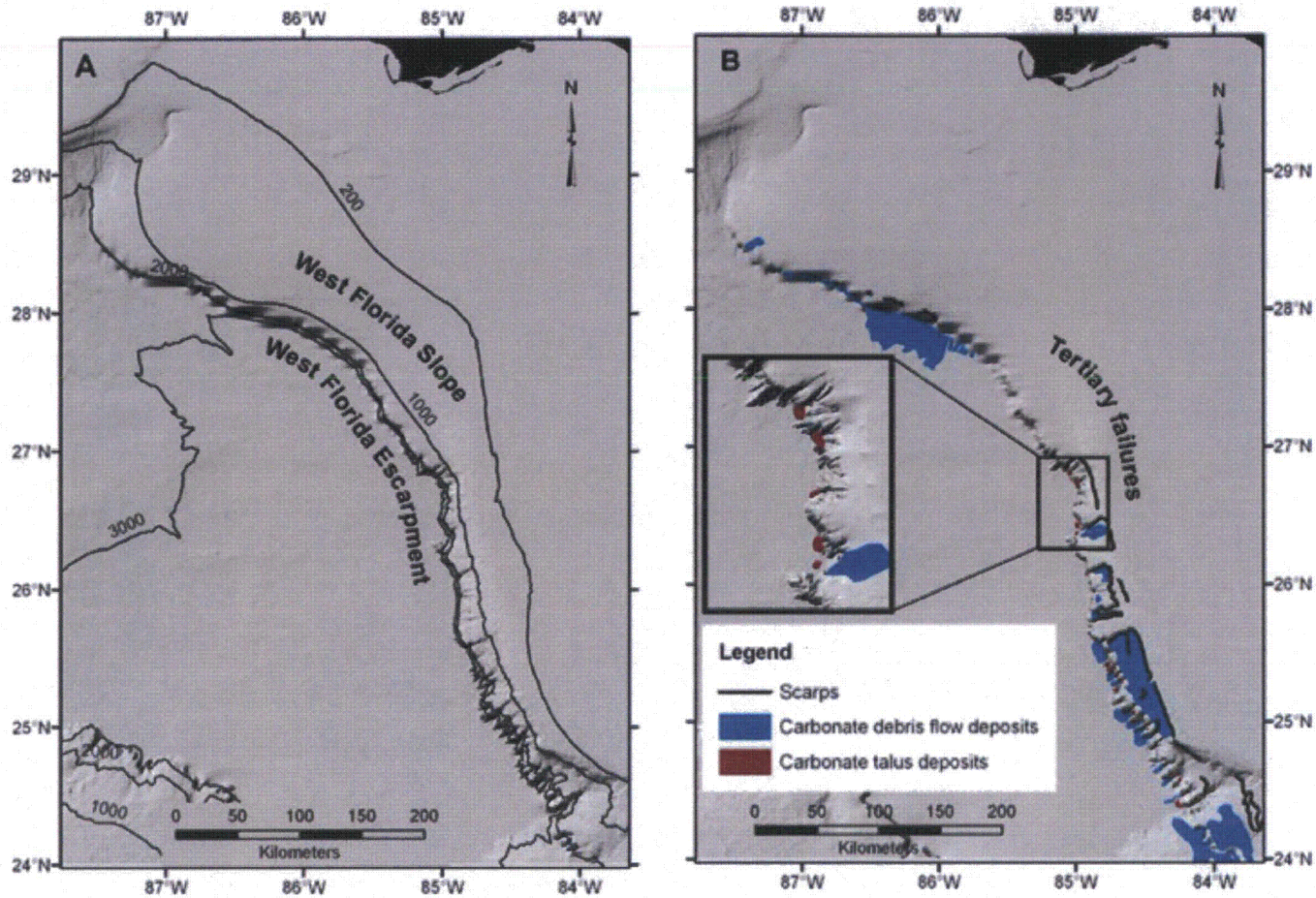

Notes:

(A) Morphology of the West Florida Escarpment and the West Florida Slope.

(B) The extent and distribution of carbonate debris flow deposits and talus deposits derived from this part of the carbonate providence. "Tertiary failures" marks general location of older land slides mapped by Mullins et al. (1986) that now have been completely buried. Inset box shows a detailed view of some of the carbonate talus deposits. Equivalent information is not available for the slope above the Campeche Escarpment.

Source:

Figure 3.2 of two USGS reports to the Nuclear Regulatory Commission (References 2.4.6-212 and 2.4.6-240)

Progress Energy Florida

Levy Nuclear Plant
Units 1 and 2
Part 2, Final Safety Analysis Report

Morphology of the West Florida Escarpment and the West Florida Slope

FIGURE 2.4.6-228 Rev 2

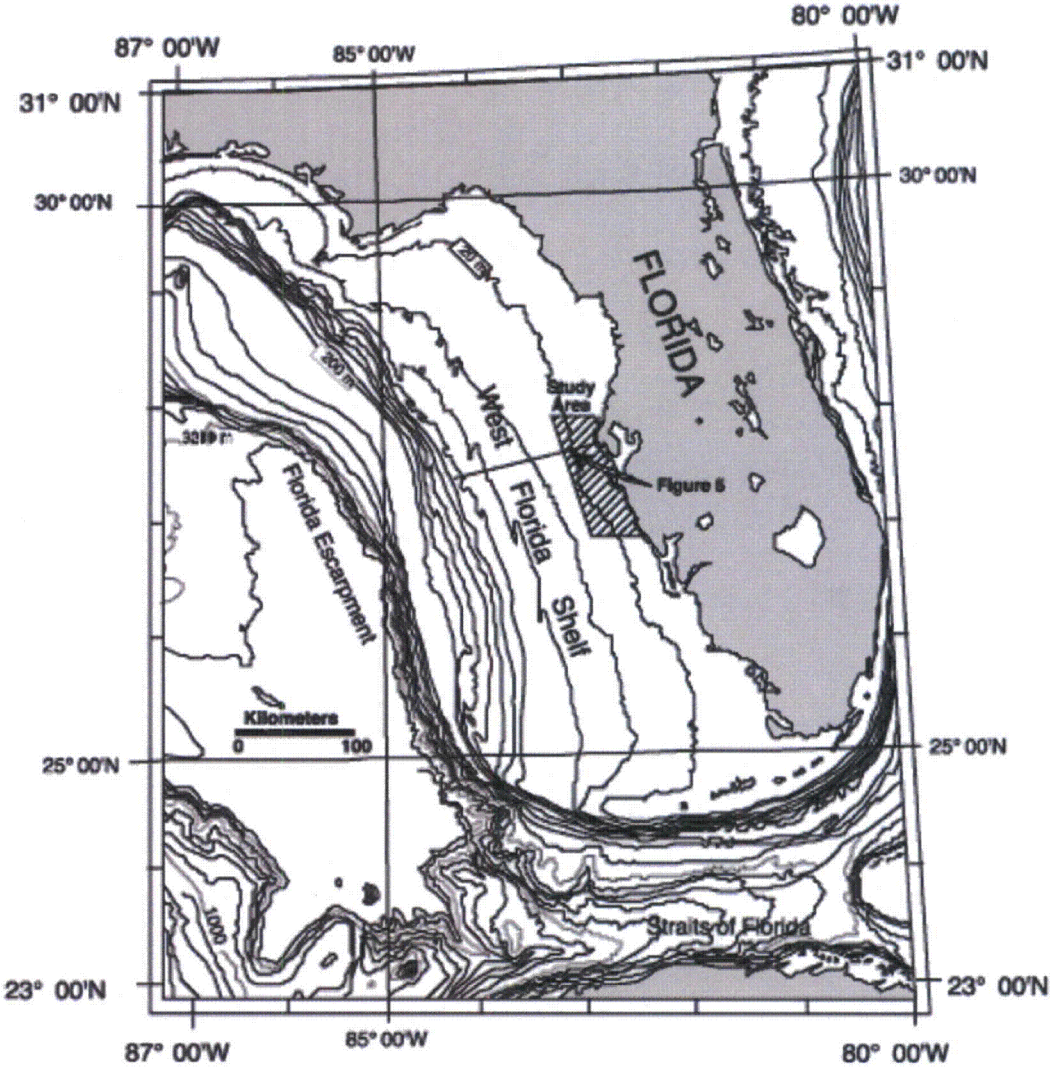

Source:
USGS, "A Summary of Findings of the West Central Florida Coastal Studies Project" Available at http://pubs.usgs.gov/of/200t/of01-303/geo!ogy.html, 2001. Accessed February 23, 2010 (Reference 2.4.6-242).

Progress Energy Florida
Levy Nuclear Plant
Units 1 and 2
Part 2, Final Safety Analysis Report

Bathymetric Map of West Florida Shelf and Slope

FIGURE 2.4.6-229 Rev 2